Aluminium foil at multiple length scales, mechanical tests and numerical simulations in Abaqus

Master's Thesis

Britta Käck
brittakaeck@gmail.com
Christoffer Malmberg
christoffer.malmberg00@gmail.com

June 25, 2015

Department of Construction Sciences
Solid Mechanics

ISRN LUTFD2/TFHF-15/5198-SE(1-82)

Aluminium foil at multiple length scales, mechanical tests and numerical simulations in Abaqus

Master's Dissertation by

Britta Käck
Christoffer Malmberg

Supervisors:
Eskil Andreasson, Tetra Pak
Per Ståhle, Professor, LTH

Examiner:
Håkan Hallberg, Associate Professor, LTH

Printed by Media-Tryck AB, Lund, Sweden
For information, address:
Division of Solid Mechanics, Lund University, Box 118, SE-221 00 Lund, Sweden
Webpage: www.solid.lth.se

Abstract

During its lifetime a beverage package is exerted to different loading conditions. Therefore an increased knowledge is needed to know how the packaging, and thus the thin layer of aluminium foil in the package, reacts to the prevailing loading scenario in a real case situation. In this thesis uni-axial tensile tests on aluminium foil samples cut out in 11 different orientations is done in order to characterize its anisotropic behaviour. To be able to reflect the behaviour of aluminium foil virtually, a material model is calibrated after key-values from the experimental results from three main orientations. To verify the material model, virtual uni-axial tensile test are executed and the results are compared with the experimental test results. The coefficient of determination between the virtual and experimental test turned out to be higher than 0.9, where 1 is a perfect fit.

Furthermore, the production process of aluminium foil seems to affect the material properties, it is further investigated how and why and later concluded that the mechanical behaviour of aluminium foil is highly dependant on the microstructure of the material.

Keywords: microstructure, Hall Petch, Hill, Ramberg-Osgood, tensile test, DIC

Work division

The main part of the presented work is made by both Britta and Christoffer. During the end of the thesis Britta focused on Digital Image Correlation while Christoffer focused on Damage mechanics simulations. Even though the final part of the thesis was divided into two parts regular briefings and discussions occurred so that both would get a better knowledge in the two subjects.

Abbreviations

RD - Roll Direction

TD - Transversal Direction

ND - Normal Direction

FCC - Face-Centered Cubic

BCC - Body-Centered Cubic

FEM - Finite Element Method

DIC - Digital Image Correlation

SEM - Scanning Electron Microscopy

FLD - Forming Limit Diagram

FLSD - Forming Limit Stress Diagram

Symbols

σ_y - Yield stress

σ_{uts} - Ultimate tensile stress

ϵ_{uts} - Ultimate tensile strain

E - Young's Modulus

W_t - Tensile absorption energy

W_f - Failure energy

Acknowledgments

We both would like to thank our families and friends for the support throughout our studies. Tetra Pak and the Division of Solid Mechanics deserves a great gratitude as well.

We would especially like to thank Tommy, Daniela, Ann-Magret, Olga, Evelina, Mathias, Andreas, Viktor and Johan for helping us with experimental testing, programs, theory and showing us what Tetra Pak do.

Thank you, Håkan, Matthias and Stephen at the Division of Solid Mechanics for support, theory, discussions and lovely DIC-testing, it was very much appreciated.

Last, but not least, a huge gratitude to our supervisors Per and Eskil who have been a constant support throughout the project. A special thanks to Eskil for providing us many interesting discussions, showing us around Tetra Pak and for all the help you have given us.

Thank you!

Contents

1 Introduction

1.1 Problem Description

The packaging material used at Tetra Pak consists of several layers, such as polymers, aluminium foil and paperboard. The aluminium foil is in the Finite Element-models described in a nonlinear elastic-plastic framework with accurate predictions in many industrial applications. However, there are some shortcomings with this approach. The material is often treated identical independent of what multi-axial stress state or strain rate that the material is exerted to. Furthermore there is limited knowledge and experience about the anisotropic material behaviour, the associated damage properties and how the properties in the smaller length scales actually affect the macro behaviour. Throughout this thesis the different length scales of aluminium foil will be discussed, these are illustrated in Fig. 1.1.

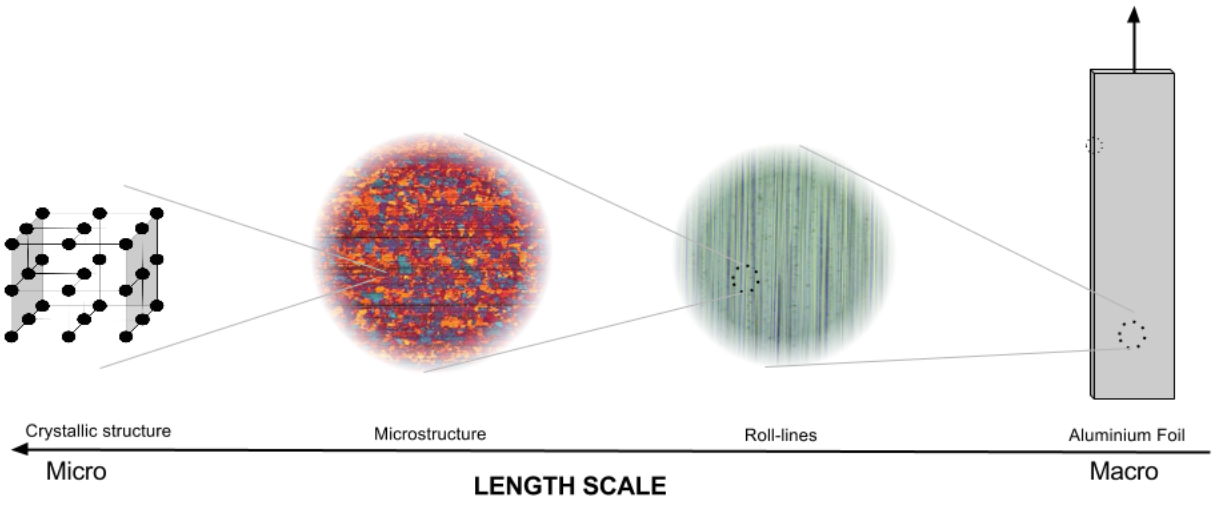

Figure 1.1: Length Scale

Background & purpose

At Tetra Pak, experimental tests on the Aluminium foil have earlier been limited to uni-axial loading in the manufacturing direction i.e Rolling Direction. A material model that reflects the anisotropic behaviour of

aluminium foil is therefore needed. Thus this thesis was initiated. The purpose of this thesis is to thoroughly characterize aluminium foil and the research is meant to be a framework for future studies of aluminium foils.

Objectives

The objectives of this projects are

- Find a suitable, simple material model that reflects the anisotropic behaviour of aluminium foil.
  - Calibrate the chosen model after orientation three main directions.
  - Validate and verify the calibrated model
- Connect the material behaviour to different length scales.
- Suggest further work for future studies.

Limitations

During this project, one type of aluminium foil with a certain thickness has been studied, implying that the results may vary for other foils. Uni-axial tensile test with monotonic proportional loading was conducted. The tests were made in a fixed climate. The material has been treated as load symmetric i.e tension and compression shows the same behaviour. No shear or multi-axial tests were performed, due to the complicity of the experimental methods. A bi-axial tensile test is the common test method to use to determine a material's anisotropic characteristics, however in this thesis it is instead chosen to do uni-axial tensile tests in one material direction at a time. Tetra Pak have developed a uni-axial tensile test method on aluminium foil that minimizes the sources of errors and from which one can acquire repeatable and trustworthy results. Therefore, in order to acquire results faster, the already developed test method was used. The results need to be validated with a bi-axial test such as a bulge test, see section *Future work*.

1.2 Ethical considerations

No ethical consideration apply to the present work.

1.3 Methodology/Approach

The focus in this master's thesis will be on performing mechanical experimental tests on aluminium foil, both on the continuum and also on the failure mechanical properties. This in order to observe and identify the deformation mechanisms and the mechanical behaviour. From the experimental results numerical material model parameters can be extracted. The model is calibrated and later on also verified with Finite Element simulations in Abaqus 6.14.

The master's thesis is divided into the following steps

- Literature study about aluminium foil production and aluminium material in general.
- Propose test methods for characterizing the mechanical and failure mechanical behaviour necessary to calibrate suitable material models in Abaqus.
- Perform experimental tests on aluminium foil in order to characterize the material behaviour.
- Calibrate the most suitable model with virtual tensile tests in Abaqus.
- Analyze and evaluate the performance of the calibrated model.

2 Aluminium foil

Since the material in focus in this thesis is aluminium foil, a thorough presentation of this widely used material is needed. In the upcoming chapter information about aluminium foil needed to understand this thesis is presented. Starting with how the foil is produced, continuing to the microstructure of the material and ending with more detailed information of the aluminium foil used in this thesis.

2.1 Overview

Aluminium foil is widely used in many industries. The reason for aluminium foils popularity is mainly due to the excellent characteristics of aluminium foil, presented below:

- Light weight
- Corrosions Resistant
- Excellent electrical and thermal conductivity.
- Malleable, Ductile
- Reflectivity
- Impermeable and odorless.

In the food packaging industry the last characteristic is especially important. If the aluminium foil would not be impermeable then the outside air would zip through the package and ruin the content.

A negative aspect of aluminium foil is that the production process of aluminium is a very high energy consuming process. However the recycling, smelting and recasting of aluminium consumes less energy and is a relatively simple process. On the contrary to other aluminium products, aluminium foil turns out to be difficult to recycle because of its thin thickness which will make it burn in the smelting process.

Due to the thickness and production process of aluminium foil the mechanical characteristics vary from bulk aluminium. This is further explained in the upcoming sections.

2.2 Production

The production of aluminium foil [Level and Federation, 1994] can be divided up into the main processes

Bauxite to Aluminium
: Alumina is extracted from the raw material bauxite through a chemical process and then turned into aluminium by the use of an electrolysis process.

Aluminium to Coil
Aluminium is hot and cold rolled into a several millimeters thick sheet and finally rolled into a coil.

Coil to Foil
The several millimeter thick sheet is rolled down to a several micrometer thick foil through a rolling, doubling and separation process.

The last two processes will be shortly described in order for the reader to better understand how every step in the production process alters the mechanical properties of the aluminium foil.

Aluminium to coil

There are two different methods that can be used in the Aluminium to Coil process, direct casting (DC) and continuous casting (CC). Depending on which is used the mechanical characteristics of the aluminium foil will vary.

Direct Casting The aluminium is directly casted into an ingot. An ingot is a large rectangular piece of a material, in this case aluminium. The ingots produced in the aluminium industry can weigh up to over 20 tons and be 500-600 mm thick, 2000 mm wide and 8000 mm long. [Level and Federation, 1994]

The ingot is reduced in thickness by a rolling process where it is rolled back and forth through metal rolls until the wanted thickness is achieved, usually in the millimeter scale. By squeezing the ingot thinner and extruding it trough the gap of the rolls, the width of the ingot is kept constant throughout the process. The results of this is a very long millimeter thick aluminium sheet rolled up as a coil.

Continuous Casting The continuous casting process, CC, is similar to DC except that instead of casting an aluminium ingot the fluid aluminium is casted into the rolling process.

The two different processes are illustrated in Fig. 2.1.

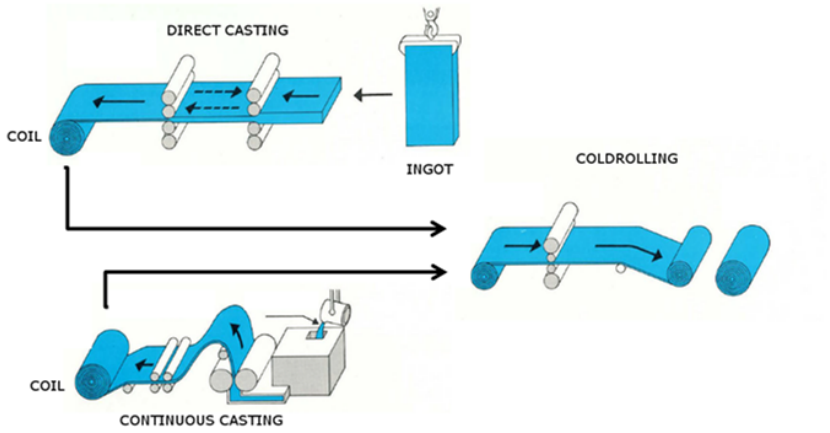

Figure 2.1: *An illustration of the DC and CC process. [Aluminiumlära (Gränges Technology Finspång)]*

Coil to Foil

After the coil has been made a reduction of thickness is needed to make the foil. A foil is defined as a sheet of materials with a thickness less than 200 μm This is achieved by another rolling process. The sheet is rolled as thin as it can be without defects in the material. Two sheets are then doubled, with rolling oil in between, and rolled again in order to make the sheets even thinner. When the wanted thickness is achieved the doubled sheet is separated, without the oil the separation would not be possible, and the foil is rolled into a coil. After the long rolling process the aluminium foil is strong but brittle, and in order to get a material that is more ductile the coil is placed into a chamber where a heat treatment called annealing is executed. This process is more thoroughly described in the microstructure section.

Alloys

Pure aluminium is rarely used since it is relatively soft. By adding alloying elements to the aluminium the wanted characteristic can be achieved. A materials characteristics depend on the major alloying element(s). Common alloying elements used are silicon (Si) and iron (Fe). [Total Materia, 2015]

2.3 Surface topography

Typically aluminium foil has one matt and one bright side, as shown in Fig. 2.2, which is an outcome from the earlier described doubling process. The bright side is the side that had contact with the smooth work roll surface and the matt side is due to the foil to foil contact during rolling. Marks from the work roll surface called roll lines, can be seen on both sides, but they are most visible on the bright side. The matt side has a more stochastic surface topography but some left over roll lines from the previous rolling can still be seen. The surface topography of the bright side is more regular and this is due to the roll-lines.

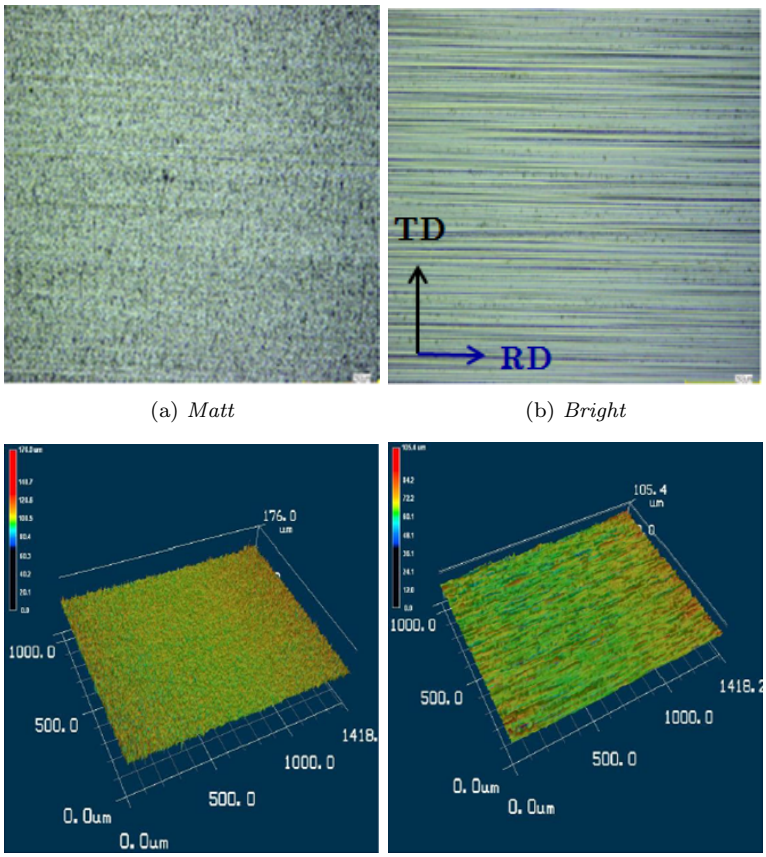

(a) *Matt* (b) *Bright*

(c) *Surface topography, matt Side* (d) *Surface topography, Bright Side*

Figure 2.2: *A micrograph and surface topography of the matt and bright side [Nasir Mehmood, Tetra Pak].*

The alloying elements in the aluminium foil is harder than aluminium. When the aluminium foil is compressed during the doubling process the harder alloying particles from one of the foils will make marks in the other foil and vice versa. This is the reason for the stochastic surface on the matt side of the foil. The alloying particles vary in thickness and the marks from larger particles will be deeper than marks from smaller particles. Thus the foil will vary in thickness. The variation of thickness due to the doubling process can be seen in Fig. 2.3.

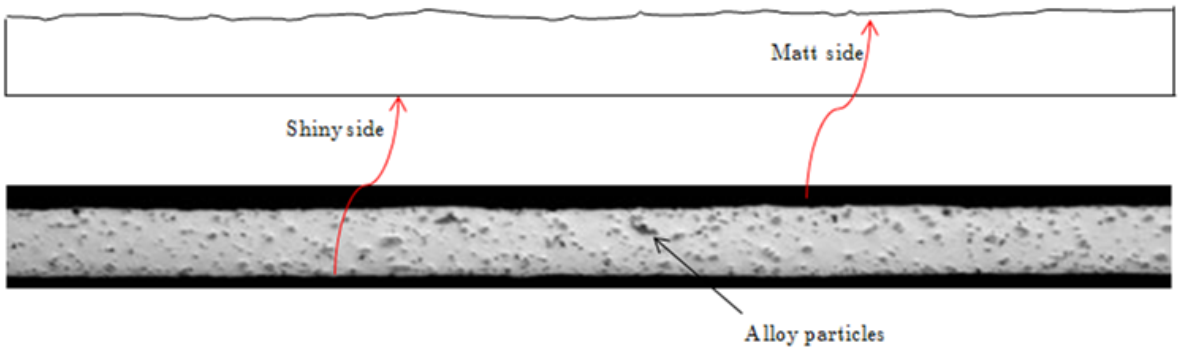

Figure 2.3: *The variation of thickness of the aluminium foil due to the foil to foil contact during the doubling process, source: external.*

2.4 Microstructure

This section will focus on the microstructure and the influence of the heat treatment of the foil in the production process.

Crystalline structure and grains

A structure of atoms that is uniquely arranged is called a crystal, i.e. a crystal follows a certain pattern. There exist several crystal systems such as cubic, tetragonal, hexagonal etc. The arrangement can be described with a three dimensional network, which is called *Space Lattice* as shown in Fig. 2.4.

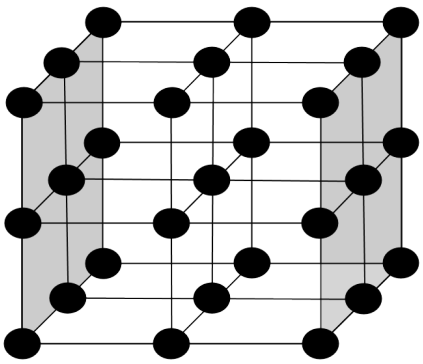

Figure 2.4: *Array of atoms, space lattice.*

In the production process, when the melted aluminium is casted and solidified, the crystals crystallize randomly and they will end up in different orientations [Callister, 2001]. A crystal with a certain orientation

is called a grain. The grains can vary in size and the interface between the grains is called grain boundary. Figure 2.5 shows how grains and their boundaries look like on a surface. The grain structure can affect the strength, hardness, ductility and formability of the material.

In the industry it is very important to understand the microstructure of a material. To predict and control the evolution of a material is the key to change the properties, in order to achieve a wanted material.

To achieve wanted characteristics of a material the key is to predict and control the evolution of the microstructure of a material in the production process.

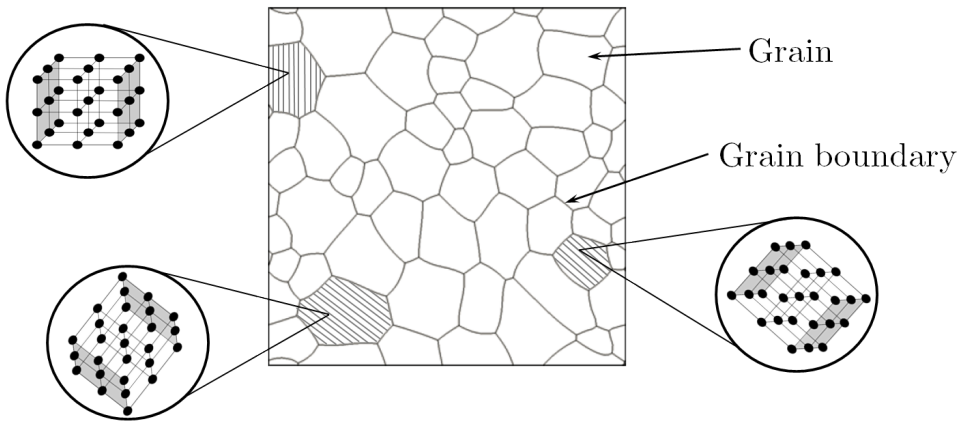

Figure 2.5: *A network of grains, the dark lines between each grain are grain boundaries [Hallberg, 2013]. The figure also show that the grains can have different orientations.*

Dislocations and grain boundaries

The crystalline structure contains structural defects, e.g. dislocations. A dislocation is defined as an irregularity in the crystalline structure. When the material is subjugated to any type of deformation the dislocations will start to move. Mechanical performance of metallic material will be influenced by movement of the dislocations.

In a deformed grain there is often different types of dislocations [Callister, 2001]. The dislocations are here denoted $\perp$ and $\top$, but can be oriented in many different ways. Under high temperatures these dislocations will move more rapidly. The dislocations $\perp$ and $\top$ will annihilate when they meet implying that the stored energy is removed. Eventually there will be a surplus of one kind after the annihilation. This surplus will start to pile up at the grain boundary, shown in Fig. 2.6.

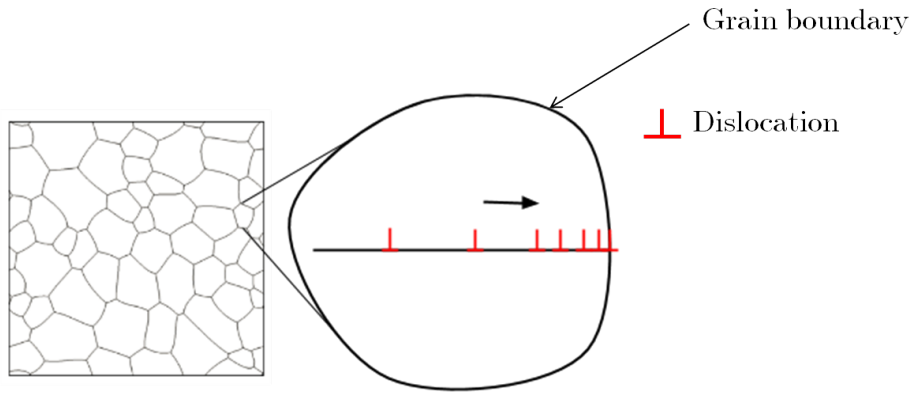

Figure 2.6: *Dislocation pile up on a grain boundary.*

Because there are many different orientations of the dislocations, all the dislocations cannot annihilate. They simply do not meet other dislocations with opposite sign. Figure 2.7 show how the density of dislocations vary in grains and grain boundaries.

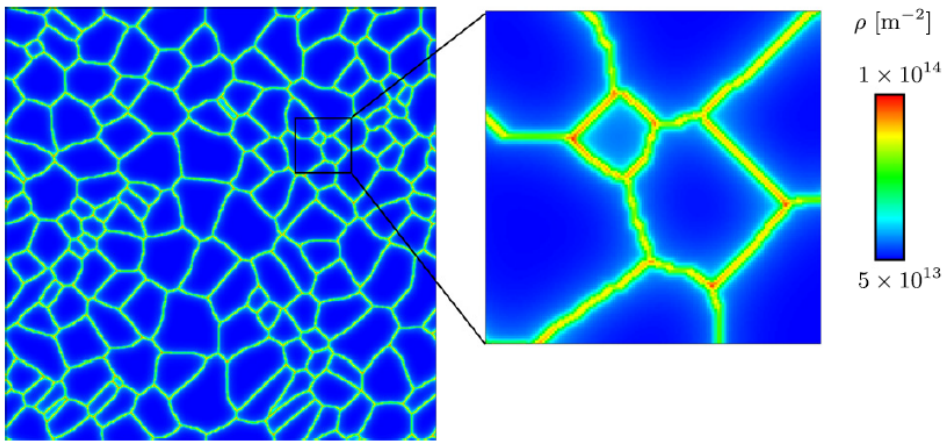

Figure 2.7: *Dislocation density in the grains [Hallberg and Ristinmaa, 2013]. It can be seen that the boundaries have larger density.*

Annealing

The physical properties of a material can be altered using a heat treatment, which is called Annealing [Callister, 2001]. The heat treatment increases the material ductility while the tensile strength decreases. Thus ductility and tensile strength are competing material characteristics. The size, orientation of the grains and the grain boundaries in the microstructure are also affected. Figure 2.8 shows how the tensile strength and ductility are influenced by an annealing process.

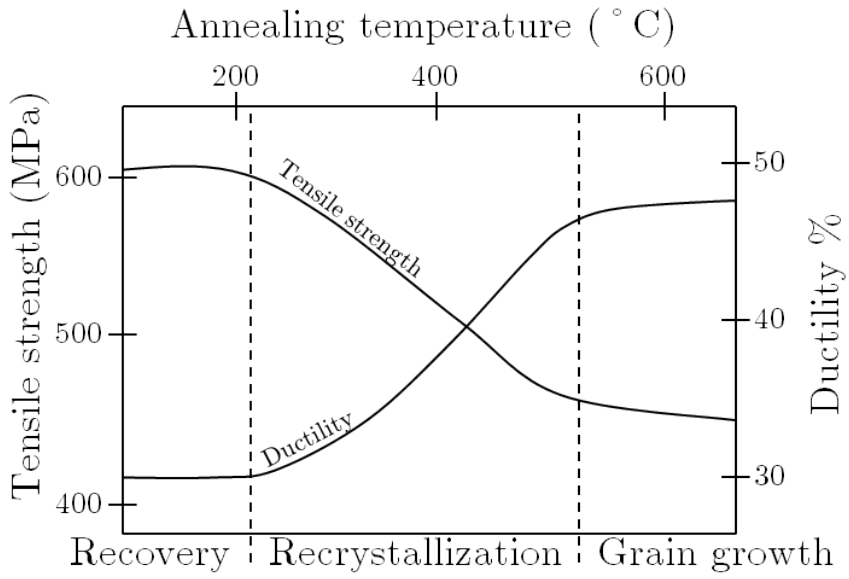

Figure 2.8: *The ductility and tensile strength are influenced by annealing temperature [Callister, 2001].*

During this process the material will reduce the stored energy received after deformation, which is often called stress relieving the material. This means that the dislocations in the material reduces. Annealing is a time and temperature dependent process and consists mainly of three stages called I) recovery, II) recrystallization and III) grain growth. Figure 2.9 shows schematically where the three stages occur during the process. The process can take up to a few days to complete, and since it is under high temperatures it needs to be in a controlled environment.

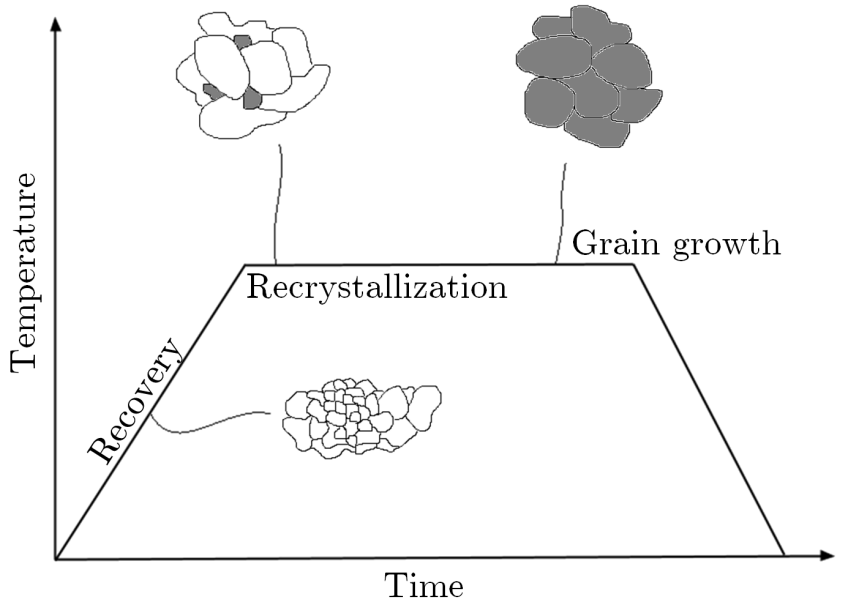

Figure 2.9: *Three stages of a full annealing cycle.*

I Recovery

The first stage of an annealing process is where defects are minimized, such as dislocations. There can be different locations in the material with more energy and other with less. This can be reflected to the grain sizes, implying that the material strives for grains to have about the same size. The material wants to level the energy so it has about the same energy throughout the material. The origin of the defects are often caused by plastic deformations of the material. By reducing the defects the material strength is reduced but the ductility increases. When the temperature is high enough the dislocations are able to move. There will be a surplus of dislocations after the annihilation of $\perp$ and $\top$ is done. The surplus tend to move into a pattern where the stored energy is reduced, which often means forming an edge that eventually will form a grain boundrary.

II Recrystallization

If a material is in a thermodynamically unstable state, a recrystallization occurs to return the material to a more stable state. In this second stage of annealing when the deformed grains are replaced by new undeformed grains, the material gets a new crystal structure. These new grains often appears on the old grain boundaries. The new grains grow more and more until they have consumed the old grains. In order to have recrystallization in an annealing process a certain temperature is often needed. Like in recovery, grain boundaries can move, however in this case boundaries with high misorientation (orientation difference between crystals) can also be moved. Figure 2.10 shows how old grains are consumed by new grains.

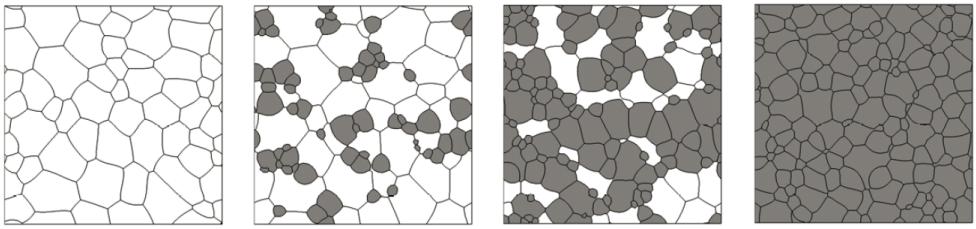

Figure 2.10: *A recrystallization process, starting from the left. In this figure we see that new grains starts to form and thereafter replacing the old grains [Hallberg, 2013].*

III Grain growth

Finally, the last stage is when the grains increase in size. The increasing grain size leads to a reduction of the total grain boundary area and thus the internal energy is decreased, implying that larger grains are weaker than smaller. The boundary movement is not continuous, the direction may change at any time. Grains can grow into other grains and the grain growth occurs by the movement of grain boundaries.

2.5 Hall Petch, Grain size

The grain size is directly connected to the yield stress of a material. This is described by the Hall-Petch relation in Eq. (2.1), where σ_0 and k are constants that depend on the material. Their values for aluminium foil are shown in Table. 2.1. [Stawovy et al., 2000]

$$\sigma_y = \sigma_0 + kd^{-1/2} \tag{2.1}$$

Table 2.1: Hall - Petch Constants

Quantity	Value
σ_0	15.7 MPa
k	2.16 MPa $\cdot mm^{1/2}$

The Hall-Petch relation for grain-sizes from 0-100 μm is shown in Fig. 2.11.

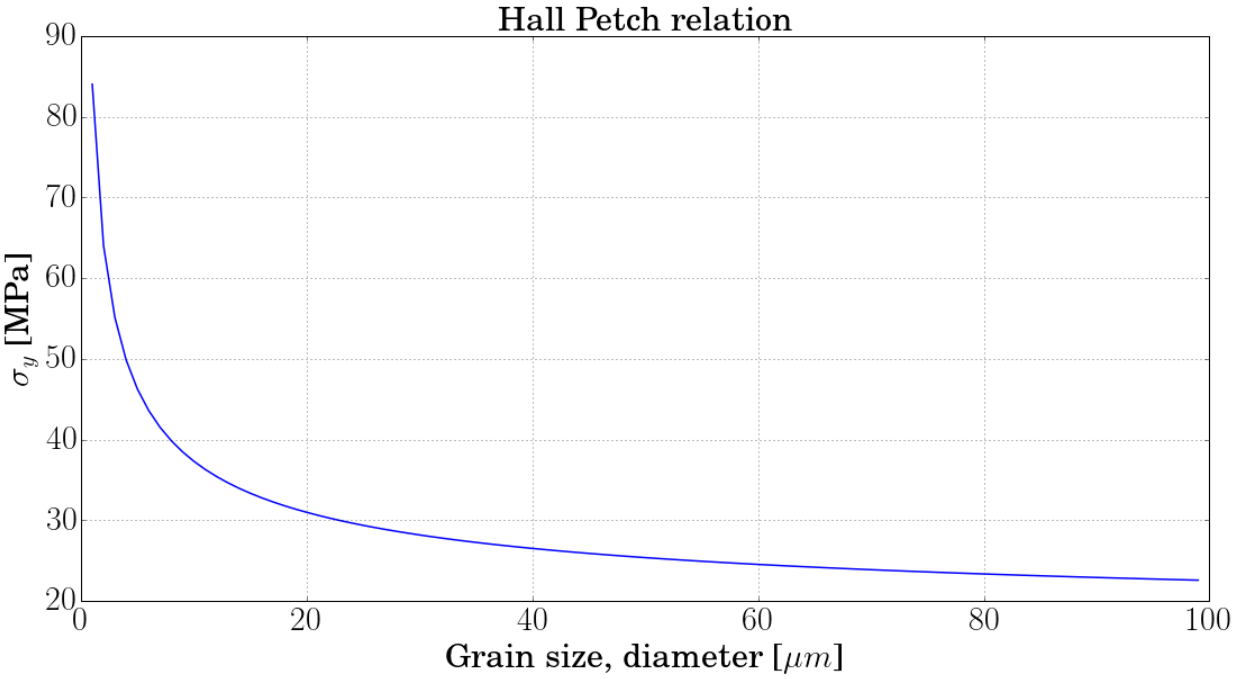

Figure 2.11: *Hall-Petch relation between the average grain size and yield stress of the material.*

2.6 The aluminium foil

In this section more specific and needed information about the aluminium foil used in this master thesis is given.

Thickness The aluminium foil is 9 μm thick, compared to household foil with a thickness of around 10-20 μm .

Alloys Iron [Fe] and Silicon [Si].

Production Method Direct Casting.

Recrystallization Not fully recrystallized, thus the foil will show anisotropic mechanical behaviour.

Grainsize 5 - 20 μm, described below.

To further investigate the recrystallization and grain size of the aluminium foil a picture of the microstructure is shown in Fig. 2.12. The grains are clearly visible and every color corresponds to a grain orientation. Black horizontal lines can be seen and these are the roll-lines, better described in Sec. 2.3 (Surface Topography). Horizontal lines of grains with the same color are visible on the sample, these are due to that the material is not fully recrystallized. A result from the cold-rolling in the production process is that the grains are pressed together and lines of grains with the same orientations evolve in the rolling direction (RD). If the material would be fully recrystallized there would not be any leftovers from this process and the material would show less anisotropic mechanical behaviour.

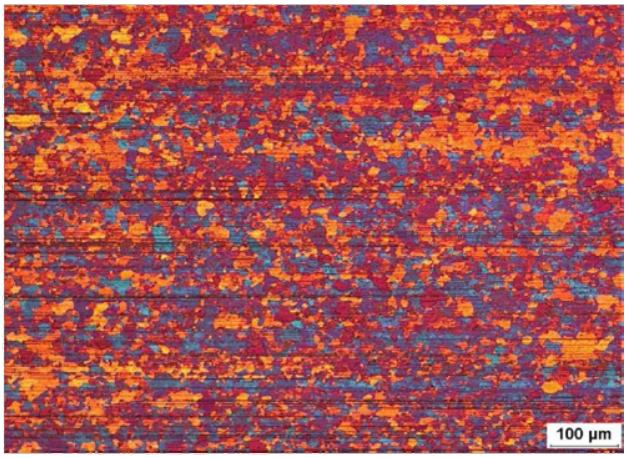

Figure 2.12: *The microstructure of the foil used in this thesis, the different colours reflect the orientation of the grains, source: external.*

The grain size varies from 5 μm to around 20 μm. Connecting the found grain size to the Hall-Petch relation in shown in Fig. 2.11 an estimated value of the yield stress for the used aluminium foil can be found, as shown in Fig. 2.13.

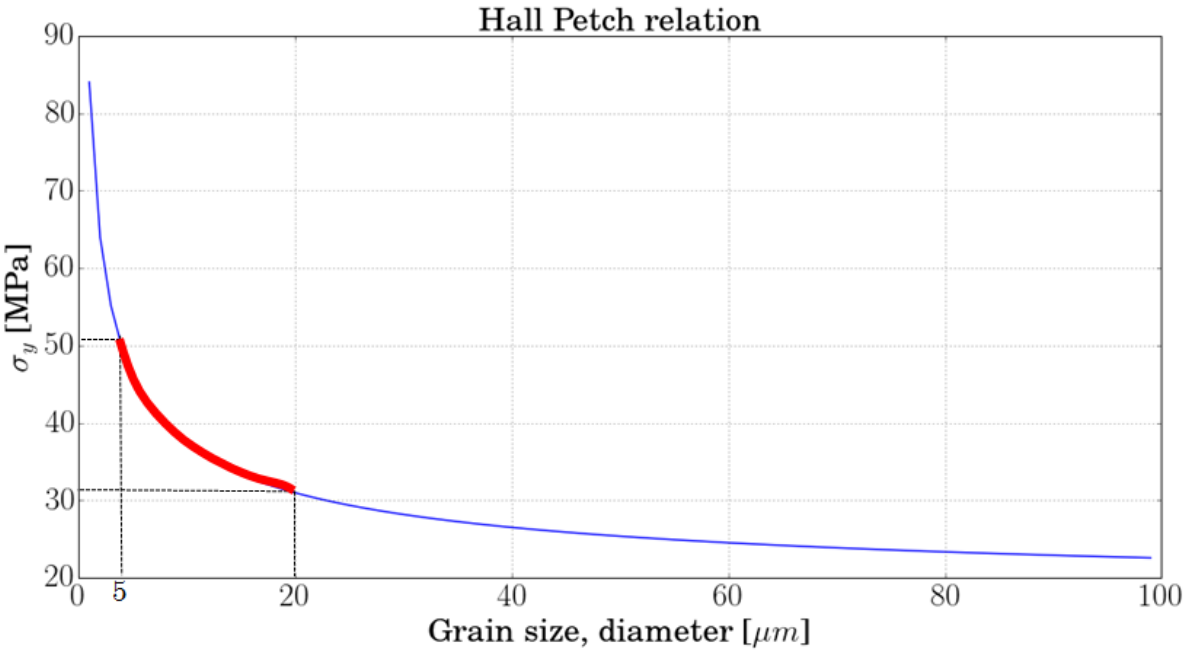

Figure 2.13: *Hall-Petch relation with predicted yield stress.*

3

Continuum and damage mechanics of aluminium foil

This chapter focuses on continuum and damage mechanics. In the continuum, elasticity and non-linear response of a material is discussed.

3.1 Elastic region

Elasticity is when a material returns to its original shape after a load. Often it is expressed with Hooke's law, i.e. $\sigma = E\epsilon$ in its most simple form. However Hooke's law can be expressed in tensor notation, that is $\boldsymbol{\sigma} = \mathbf{C}\boldsymbol{\epsilon}^e$. For an orthotropic material in plane stress condition it can be expressed as in Eq. (3.1) [Mäkelä and Östlund, 2003] if the main material directions coincide with the 1, 2 and 3 directions. Orthotropic symmetry will be discussed under section 3.2.

$$\boldsymbol{\sigma} = \begin{bmatrix}\sigma_{11}\\ \sigma_{22}\\ \sigma_{12}\end{bmatrix} = \frac{1}{1-\nu_{12}\nu_{21}}\begin{bmatrix}E_1 & \nu_{21}E_1 & 0\\ \nu_{12}E_2 & E_2 & 0\\ 0 & 0 & G_{12}(1-\nu_{12}\nu_{21})\end{bmatrix}\begin{bmatrix}\epsilon^e_{11}\\ \epsilon^e_{22}\\ 2\epsilon^e_{12}\end{bmatrix} = \mathbf{C}\boldsymbol{\epsilon}^e$$
$$\epsilon_{33} = -\Big(\frac{\nu_{13}\sigma_{11}}{E_1} + \frac{\nu_{23}\sigma_{22}}{E_2}\Big) \tag{3.1}$$

where E is Young's modulus, ν Poisson's number and G is the shear modulus. Aluminium foil is actually in a 3D configuration but it can be reduced to a 2D configuration with an assumption. The assumption can be plane stress or plane strain. Plane stress is when the normal stress to the 1-2 plane, i.e. the stress perpendicular to the 1-2 plane, is assumed zero. Plane strain, in a similar way for plane stress, is when the normal strain to the 1-2 plane is assumed to be zero. Plane stress can be used when the thickness is much smaller than the width and height of the specimen. Plane strain can be used when the thickness is much larger than the width and height. Figure 3.1 shows these two types. Since the thickness of the aluminium foil is much smaller than the height and width, plane stress is assumed for this thesis.

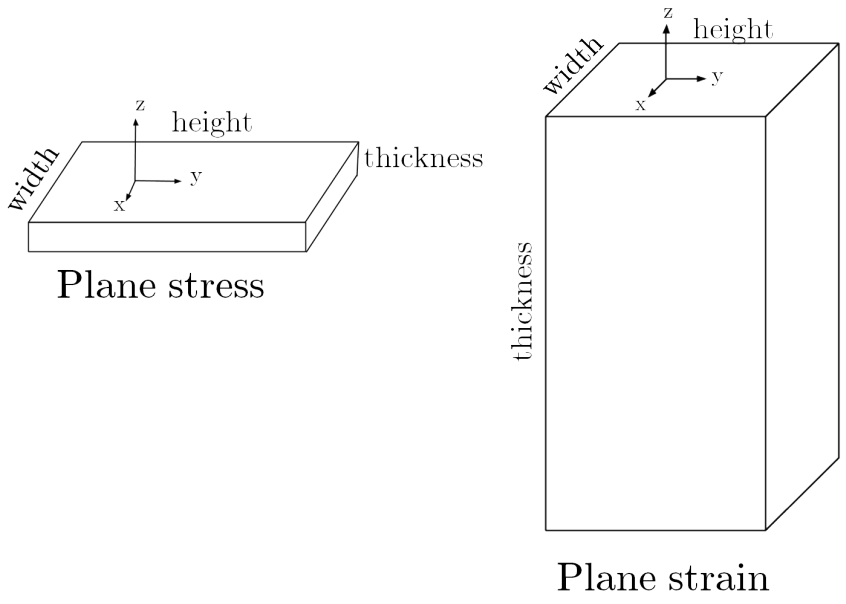

Figure 3.1: *A figure illustrating Plane stress and Plane strain.*

3.2 Non-linear material response

This section will focus on non-linear behaviour of a material. With a single analytical expression it is possible to explain the continuum of a material response. Furthermore, it can be combined with another model to explain the evolution of the material responses. The theory in this section considers a uni-axial load case.

Analytical expression combined with evolution

The mechanical response of aluminium exhibits a smooth continuous non-linear curve. This stress-strain curvature can for instance be approximated by the, often used, analytical Ramberg-Osgood Eq. (3.2) [Ramberg and Osgood, 1943]. The Ramberg-Osgood model is usually used for paper but its curvature reflects aluminium foils behaviour as well, which is shown in Fig. 3.2.

$$\epsilon = \frac{\sigma}{E}\Big(1 + \alpha\Big(\frac{\sigma}{\sigma_0}\Big)^{n-1}\Big) \quad n > 1 \tag{3.2}$$

where α and n are dimensionless parameters.

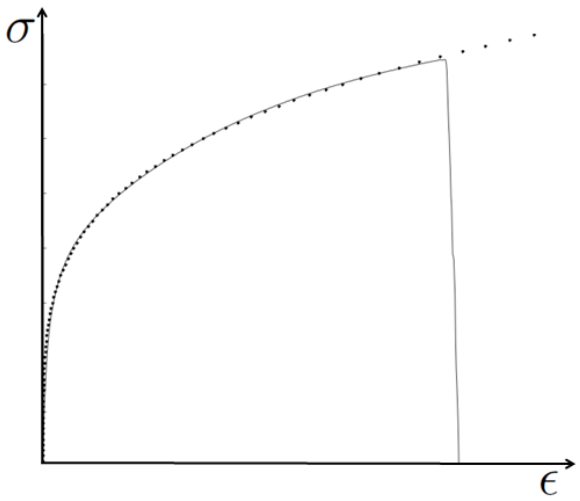

Figure 3.2: *A typical uni-axial tensile test curve for aluminium foil and the analytical Ramberg-Osgood model. The curvature of the analytical model reflects the behaviour of aluminium foil very well.*

In order to use Eq. (3.2) some guessing has to be made for the parameters α and n, which can be complicated. Another method is to rewrite Eq. (3.2) into Eq. (3.3) and quantify the design parameters by using the definition of tensile energy absorption.

$$\epsilon = \frac{\sigma}{E} + \left(\frac{\sigma}{E_0}\right)^N \tag{3.3}$$

In the above Eq., E_0 is the strain-hardening modulus and N is the strain-hardening exponent [Mäkelä, 2012]. The curvature is shown in Fig. 3.2. From a simple tensile test it is possible to quantify four parameters which are the Young's modulus E, ultimate tensile strength σ_{uts}, ultimate tensile strain ϵ_{uts} and the tensile energy absorption W_t. The tensile energy absorption is defined as

$$W_t = \int_0^{\epsilon_{uts}} \sigma d\epsilon$$

which can be rewritten to

$$W_t = \sigma_{uts}\epsilon_{uts} - \int_0^{\sigma_{uts}} \epsilon d\sigma = \sigma_{uts}\epsilon_{uts} - \frac{\sigma_{uts}^2}{2E} - \frac{\sigma_{uts}^{N+1}}{(N+1)E_0^N} \tag{3.4}$$

where the integral was calculated by using Eq. (3.3). By rewriting Eq. (3.3) to

$$E_0^N = \frac{\sigma_{uts}^N}{(\epsilon_{uts} - \sigma_{uts}/E)} \tag{3.5}$$

and use it in Eq. (3.4) the tensile energy absorption can be written as

$$W_t = \sigma_{uts}\epsilon_{uts} - \frac{\sigma_{uts}^2}{2E} - \frac{\sigma_{uts}(\epsilon_{uts} - \sigma_{uts}/E)}{(N+1)}$$

Now, the strain-hardening exponent can be expressed by the quantities given by the tensile test such as

$$N = \frac{\sigma_{uts}^2 - 2EW_t}{\sigma_{uts}^2 + 2E(W_t - \sigma_{uts}\epsilon_{uts})} \tag{3.6}$$

The strain-hardening modulus can be obtained by using Eq. (3.5)

$$E_0 = \frac{\sigma_{uts}}{(\epsilon_{uts} - \sigma_{uts}/E)^{\frac{1}{N}}} \tag{3.7}$$

With equations (3.3), (3.6) and (3.7) it is simple to quantify a curve that fits the experimental curve.

Consider an uni-axial loading curve, see Fig. 3.3. In this case the material behaves linear elastic with Young's modulus E until it reaches the point at which it starts to yield, σ_y. Continue to load the material to point A and then unload to point B, the material has been permanently deformed. This is plastic deformation. Loading the material again it will behave linear elastic with the same Young's modulus up to the point A, which is the new yielding point of the material. Continue to load it and the material will follow the same path towards C as if the unloading at point A have never occurred.

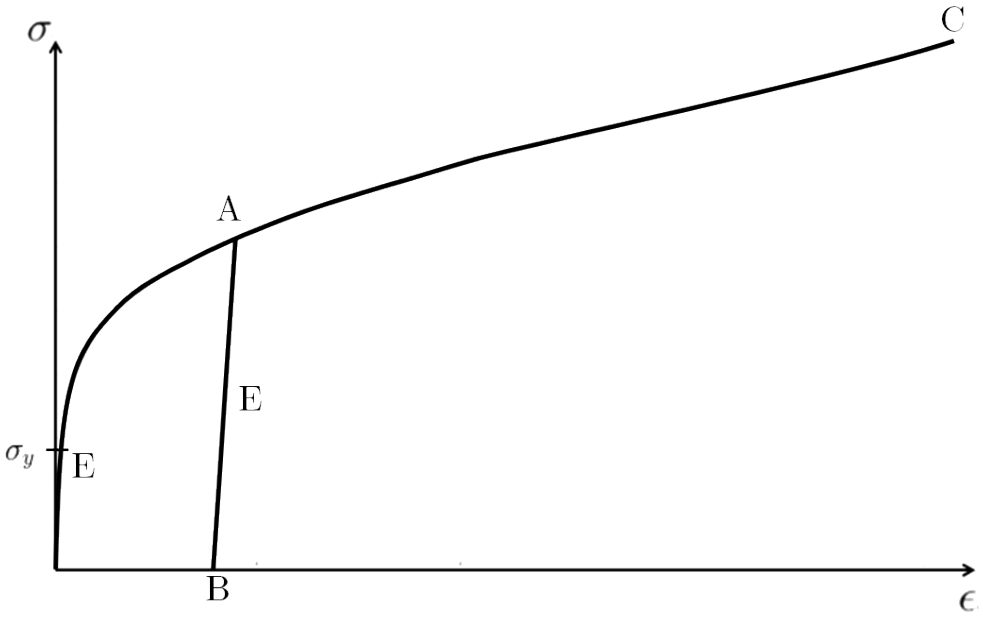

Figure 3.3: *Stress and strain curve for an uni-axial loading*

The yield stress increases for every load and unload scenario after point A, a hardening effect has arisen. At some point the loading will reach a maximum stress, or failure stress. In some cases, for example in a conventional program if one only have data to a certain point, the program assumes a perfect plasticity. In other cases it continuously hardens. Figure 3.4 shows these behaviors.

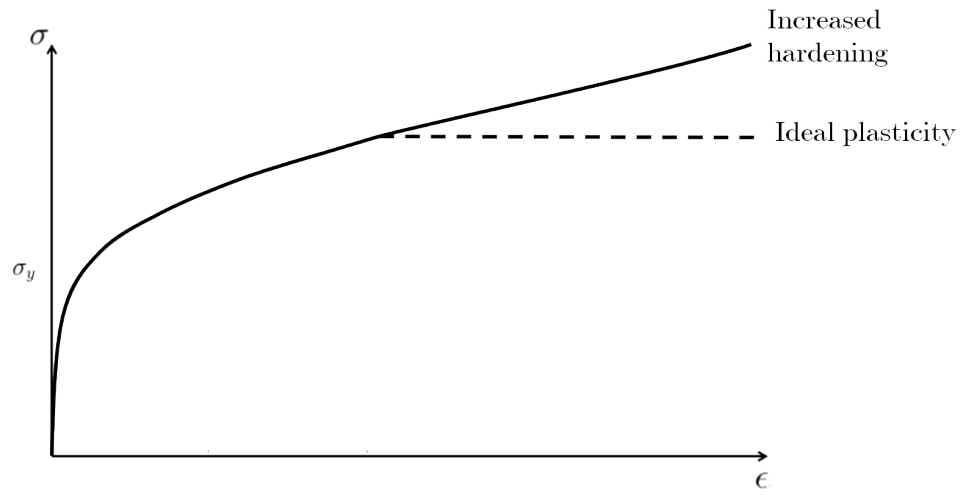

Figure 3.4: *Stress and strain curve followed by ideal plasticity and increased hardening.*

One way to predict material responses is to study a yield surface. To start with, consider a yield surface for an isotropic material. von Mises criterion expressed in principal stresses in 3-dimensional configuration can be expressed as

$$\frac{1}{2}\Big((\sigma_1 - \sigma_2)^2 + (\sigma_1 - \sigma_3)^2 + (\sigma_2 - \sigma_3)^2\Big) = \sigma_{y0}^2$$

where σ_1, σ_2 and σ_3 are principal stresses and σ_{y0} is yield stress for the material. In a similar manner this can be written for a failure surface. On the contrary from failure mechanics theory, in which an existing and postulated failure is regarded, it is here assumed that the failure is an isotropic and continuously distributed damage. Figure 3.5 shows how to fit yield and failure points into surfaces.

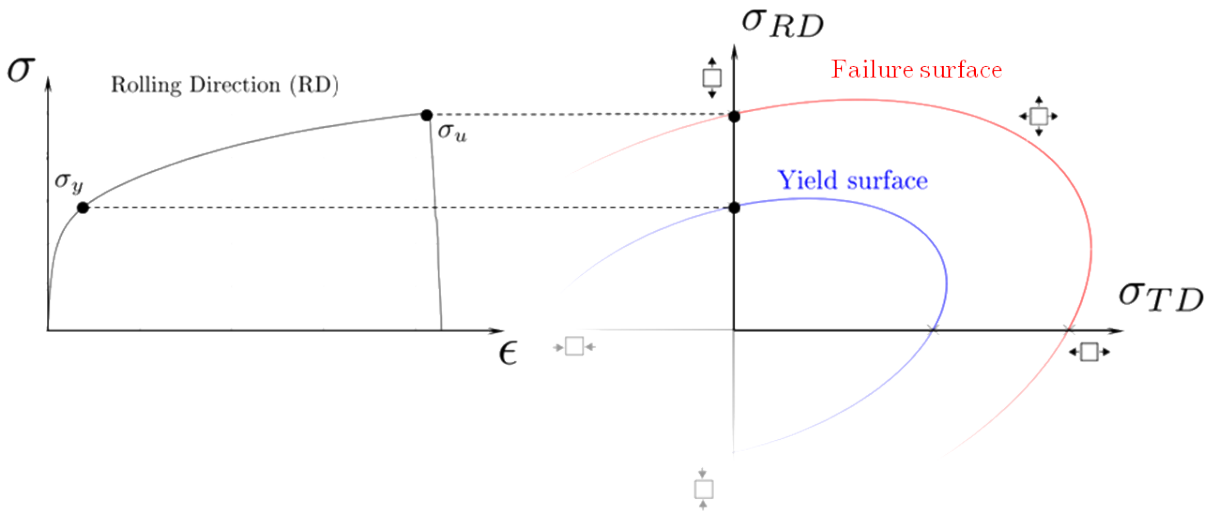

Figure 3.5: *With the associated yield surface and the subsequent evolution of the yield surface, i.e. failure surface.*

Calibration of Hill's yield criterion

Orthotropic Hill criterion [Hill, 1948] can be expressed as

$$f = F(s_{22} - s_{33})^2 + G(s_{33} - s_{11})^2 + H(s_{11} - s_{22})^2 + 2Ls_{23}^2 + 2Ms_{13}^2 + 2Ns_{12}^2 = 1 \tag{3.8}$$

In a uni-axial load case, where it is assumed that the out of plane deformations is negligible, Hill's orthotropic yield criterion, Eq. (3.8), can be rewritten into Eq. (3.9) in the 1-2 plane ($s_{33} = s_{23} = s_{13} = 0$).

$$f_{1,2}(s_{11}, s_{22}, s_{12}) = Gs_{11}^2 + Fs_{22}^2 + H(s_{11} - s_{22})^2 + 2Ns_{12}^2 = 1 \tag{3.9}$$

Expressing the yield criteria in experimentally measured values, a transformation of stresses is requires. s_α is the measured yield stress in the α direction from a uni-axial tensile test. The transformation is more thoroughly described in Appendix B.

$$\begin{aligned} s_{11} &= s_\alpha cos^2(\alpha) \\ s_{22} &= s_\alpha sin^2(\alpha) \\ s_{12} &= s_\alpha sin(\alpha)cos(\alpha) \end{aligned}$$

By inserting the above expressions into Eq. (3.9) and solve for s_α, the yield stress value is found for every direction. This value is represented in the material directions, i.e. RD and TD configuration, and therefore can be compared with the other directions.

$$s_\alpha = 1/\sqrt{(F+H)cos^2(\alpha) + (G+H)sin^2(\alpha) + 2(N-H)cos(\alpha)sin(\alpha)}$$

In order to solve the Eq. above the variables need to be determined. First, the same transformation as above is done for three angles, 0°, 45° and 90° which will give three different load cases, shown in Table. 3.1. 0° is defined as RD and 90° is defined as TD.

Table 3.1: Stress Transformation

	α=0	α=45	α=90
$s_{11} = s_\alpha cos^2(\alpha)$	s_0	$\frac{1}{2}s_{45}$	0
$s_{22} = s_\alpha sin^2(\alpha)$	0	$\frac{1}{2}s_{45}$	s_{90}
$s_{12} = s_\alpha sin(\alpha)cos(\alpha)$	0	$-\frac{1}{2}s_{45}$	0

Insertion of the transformed variables in Eq. (3.9) results in the relations below are acquired.

$$f_{1,2}(s_0, 0, 0) = (G + H)s_0^2 = 1$$

$$f_{1,2}(0, s_{90}, 0) = (F + H)s_{90}^2 = 1$$

$$f_{1,2}(-\frac{1}{2}s_{45}, -\frac{1}{2}s_{45}, -\frac{1}{2}s_{45}) = (F + G + N)s_{45}^2 = 4$$

To determine the constants, F, G, H, N, another criterion is needed (Above: 4 unknown and 3 equations). The material is postulated as transverse isotropic in these derivations, $s_{22} = s_{33}$ and $s_{12} = s_{13}$. Hill's yield criterion expressed in plane stress in the 1-3 plane is

$$f_{1,3}(s_{11}, s_{33}, s_{13}) = Fs_{33}^2 + Hs_{11}^2 + G(s_{11} - s_{33})^2 + 2Ms_{13}^2 = 1$$

and using that $s_{22} = s_{90} = s_{33}$ the Eq. below is found.

$$f_{1,2}(0, s_{90}, 0) = f_{1,3}(0, s_{90}, 0) = (F + G)s_{90}^2 = 1$$

This mean that there is four equations and four unknown variables, thus the system can be solved.

$$\begin{aligned}
&(G + H)s_0^2 = 1 && G = \frac{1}{2s_0^2} \\
&(F + H)s_{90}^2 = 1 && H = G = \frac{1}{2s_0^2} \\
&(F + G + N)s_{45}^2 = 4 && F = \frac{1}{s_{90}^2} - \frac{1}{2s_0^2} \\
&(F + G)s_{90}^2 = 1 && N = \frac{2}{s_{45}^2} - \frac{1}{2s_{90}^2}
\end{aligned} \tag{3.10}$$

The yield surface is now calibrated after yield stress values measured in three directions.

R-Values

In order to reflect the anisotropic behaviour of the aluminium foil in a virtual model in Abaqus, the anisotropic yield stress values, R-values, need to be calculated [Abaqus, 2015]. In Abaqus these are introduced as stress-ratios that are applied in Hill's potential function (3.8). The R-values are defined in Table. 3.2.

The R_{12} (= R_{13}) expression is found by expressing s_{12} in the variable N and then using the relation for $N(s_{45}, s_{90})$ in (3.10), the calculations are described in (3.11).

$$
\begin{aligned}
f_{1,2}(0,0,s_{12}) &= 2Ns_{12}^2 = 1 \\
s_{12} &= \sqrt{\frac{1}{2N}} \\
\text{where } N &= \frac{2}{s_{45}^2} - \frac{1}{2s_{90}^2} \\
s_{12} &= \sqrt{\frac{1}{\frac{4}{s_{45}^2} - \frac{1}{s_{90}^2}}}
\end{aligned}
\tag{3.11}
$$

Table 3.2: Normalized R-values, Potential input in Abaqus.

R-values	Definition	Definition with experimental values
R_{11}	$\frac{\tilde{\sigma}_{11}}{\sigma^o}$	$\frac{s_0}{s_0}$
R_{22}	$\frac{\tilde{\sigma}_{22}}{\sigma^o}$	$\frac{s_{90}}{s_0}$
R_{33}	$\frac{\tilde{\sigma}_{33}}{\sigma^o}$	$\frac{s_{90}}{s_0}$
R_{12}	$\frac{\sqrt{3}\tilde{\sigma}_{12}}{\sigma^o}$	$\frac{\sqrt{3}}{\sigma^o}\sqrt{\frac{1}{\frac{4}{s_{45}^2} - \frac{1}{s_{90}^2}}}$
R_{13}	$\frac{\sqrt{3}\tilde{\sigma}_{13}}{\sigma^o}$	$\frac{\sqrt{3}}{\sigma^o}\sqrt{\frac{1}{\frac{4}{s_{45}^2} - \frac{1}{s_{90}^2}}}$
R_{23}	$\frac{\sqrt{3}\tilde{\sigma}_{23}}{\sigma^o}$	$\frac{\sqrt{3}s_{90}}{s_0}$

3.3 Material failure theory

The focus of this section is to describe two criteria for later use in virtual testing.

There exist many different types of material failure theories, however this thesis is limited to two simplified material failure criteria, Forming Limit Diagram (FLD) and Forming Limit Stress Diagram (FLSD). FLD is a strain based criterion. In order to get the data points for the Forming Limit Curve, one needs to determine the strain in the 1-direction and the 2-direction as shown in Fig. 3.6. These two directions represent the *major* and *minor* strains respectively in the criterion. A simplification that can be made is to use only one point of the FLD diagram. By setting the minor to 0 and the major to the wanted strain, the spot where the material breaks is acquired, independent of direction. FLSD works in a similar way as FLD, but it uses stress instead of strain.

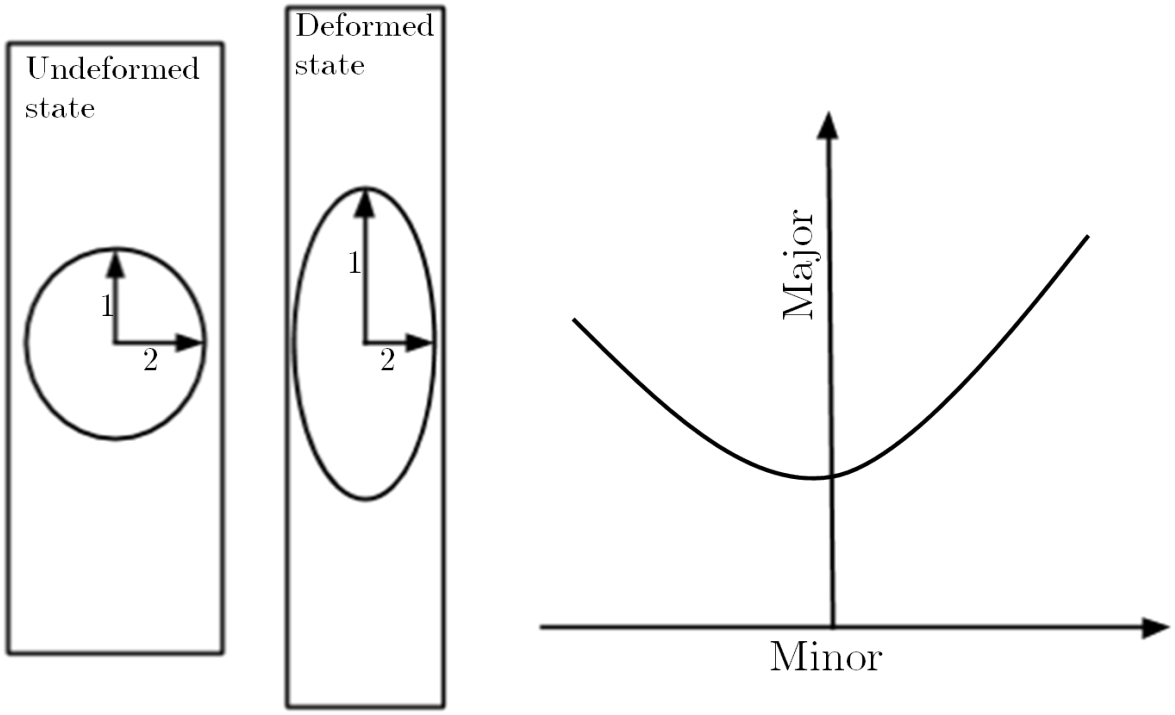

Figure 3.6: *A simple figure defining the direction of the FLD and FLSD criteria. To the right is a representative diagram for the two criteria.*

In the graph to the right in Fig. 3.6 shows how a FLD diagram may look like. For a uni-axial test the minor strain decreases but the major strain increases, which is illustrated to the left in Fig. 3.6. This is also illustrated in the graph in Fig. 3.6. Naturally for a multi-axial test, e.g. bi-axial test, both the major and minor increases with increased strain. To use this criterion it is needed to compare the current strain with the reference strain, where current is where the test is at and reference is the curvature. If the current strain is under the curve there is no damage and if above implies that damage has occurred.

4 Experimental methods

In this chapter the experimental and imaging methods used in this thesis are presented. One of the most common experimental methods is the tensile test. From this a basic macro - mechanical characterization can be made. If it is interesting to see local deformations of a sample in-situ, Digital Image Correlation (DIC) is the imaging technique to turn to. DIC makes it possible to investigate and evaluate the local behaviour in a macroscopic test.

4.1 Tensile test

A tensile test can be executed to determine the basic mechanical characteristics and properties of a material. A tensile test can be either uni-axial, applied force along one axis, or bi-axial, applied force along two axis simultaneously. Uni-axial tensile test is most common and is often sufficient enough. A bi-axial tensile test is mainly used to determine anisotropic behaviour of a material. However bi-axial testing on Aluminium-foil is complicated and results in many sources of errors. The anisotropic behaviour can also be studied by doing uni-axial tensile tests on samples cut out in different directions from one material. Since this is a relatively simpler and thrust worthy method only uni-axial tensile tests have been executed in this thesis.

A simple sketch of the basic setup of a typical tensile testing machine is shown in Fig. 4.1. The machine basically pulls the mounted sample until failure and registers the force on the top boundary and the change in displacement of the top grip. Results from a tensile tests are typically shown in a force vs displacement graph or converted into a stress vs strain graph.

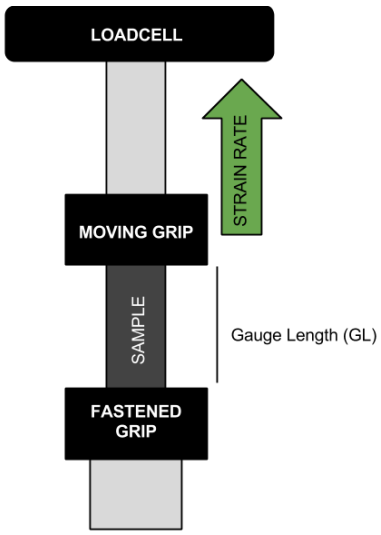

Figure 4.1: *The basic setup of a typical Uni-axial Tensile testing machine.*

4.2 Digital Image Correlation

If pictures of a sample are taken continuously throughout an experimental process the displacement in the sample can be identified by comparing the pictures. This is done with Digital Image Correlation, DIC, a full-field image analysis method. Particles or fragments, on the sample are chosen in the reference picture and then identified on the deformed picture. By doing this the mapping from the reference picture to the deformed can be identified for that specific fragment or particle. If the mapping for all fragments or particles is done from one image to another a displacement field over the sample is acquired. Thus information about local and global strain distribution is acquired.

The sample of the material must have a texture so that every fragment have a uniqueness. The pattern must follow the movement of the material and the speckle can not be too small because it has to be resolved by the image. If there are larger homogeneous spots these must be smaller than the fragment used in the correlation. Some materials have a natural pattern but if the sample is, for example, aluminium foil, a speckle pattern must be applied [Schreier et al., 2009]. The DIC method is illustrated in Fig. 4.2.

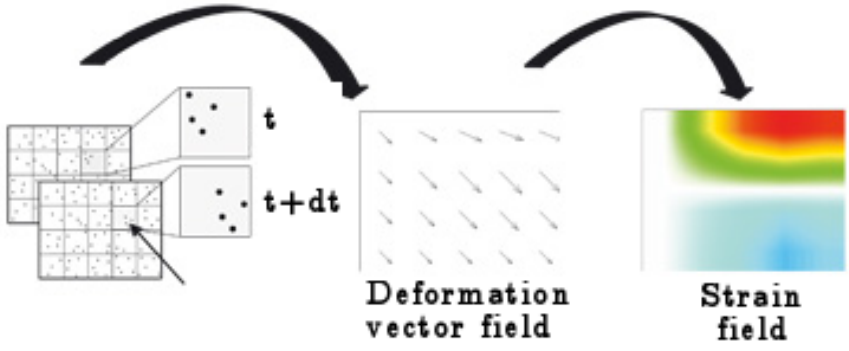

Figure 4.2: *Digital Image Correlation, the fragments are tracked from one time to another and from this a displacement vector field is acquired. The deformation vector field can then be converted into a strain field [LaVision, 2010].*

5 Experimental tensile tests

In this thesis three different uni-axial tensile test setups, all with its purpose, have been performed on aluminium foil samples. The purpose of the first test was to find the complete mechanical characteristics in different material orientations and to study the anisotropic behaviour of aluminium foil. The second tests were performed to examine the deformation process and the accompanied crack initiation and failure behaviour of aluminium foil. In order to better study how the deformations in a sample evolve and localizes in a process, the final tensile test with a DIC system was executed to investigate the local deformation.

5.1 Mechanical and anisotropic behaviour, Test1

In order to thoroughly study the mechanical material behaviour of aluminium foil a tensile test, see section 4.1, was carried out on aluminium foil samples cut out in different directions. Eleven directions were examined which are illustrated in Fig. 5.1

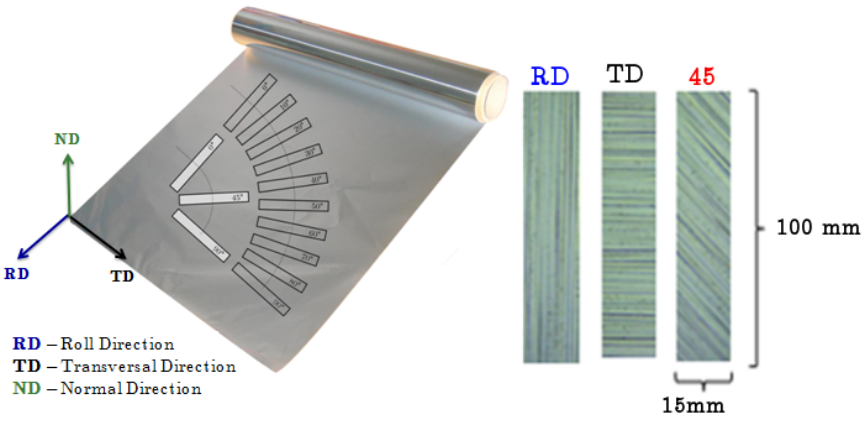

Figure 5.1: *The samples were cut out from the foil sheet in different directions, as illustrated. 0 ° is defined as RD and 90 ° is defined as TD*

First rectangular samples (200x25 mm) were cut out from an aluminium foil sheet with a sharp rounded scalpel. A preparation of 15 samples in every direction were made, shown in Fig. 5.2a. The samples were

thereafter cut again with a more precise and sharp double cutter, shown in Fig. 5.2b into the size (200x15 mm) and red tape was applied on the edges with a distance of 100 mm apart. This is shown in Fig. 5.2c. The gauge length is equal to the distance between the tape, the sample is mounted into the tensile tester so that the tape is not visible, shown in Fig. 5.2d. When all the samples were prepared the five best samples (no visible cracks or holes) were chosen and the tensile tests were executed. The tensile test was performed with an Instron tensile tester with 50 mm wide and smooth rubber grips and a 100 N load cell.

(a) *Samples cut out from the foil sheet in one direction*

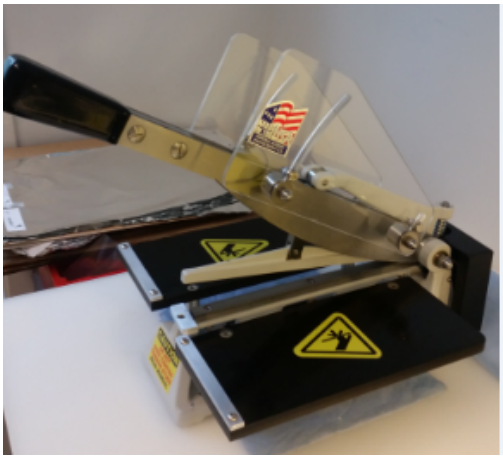

(b) *Double Cutter, cuts the sample's width to 15 mm*

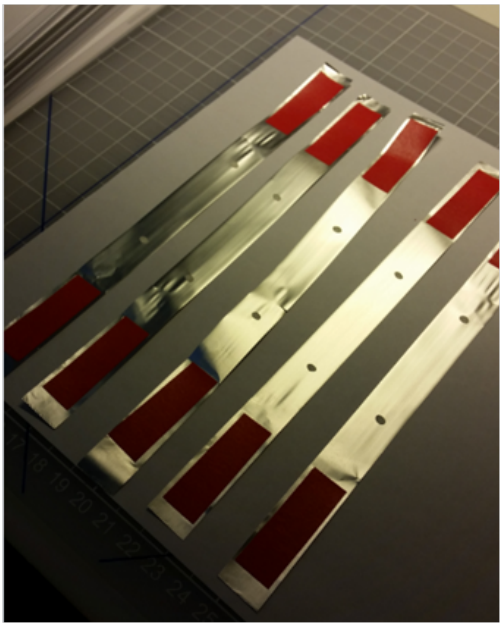

(c) *Prepared samples, cut in the Double cutter and taped*

(d) *Mounted sample, no tape outside of the fastened grips*

Figure 5.2: *Sample preparation and setup.*

The tests were carried out with a strain rate of 9 mm/min and a preload of 0.2 N. From every tensile test force and displacement data was acquired, plotted and analyzed. From the tensile test data some material characteristics could be identified, how these were determined is described in Fig. 5.3. Young's modulus, E is the slope on the dotted line shown in the Fig.. The ultimate tensile stress σ_{uts} and the ultimate tensile strain ϵ_{uts} is the maximum strain and stress before break. The yield stress, σ_y, is the stress-value where the material starts to yield. Tensile absorption energy, W_t is the shaded area and the failure energy, W_f, is area under the failure part of the curve. The results from this test method are both reproducible and repeatable, therefore fewer tests samples was made in Test2.

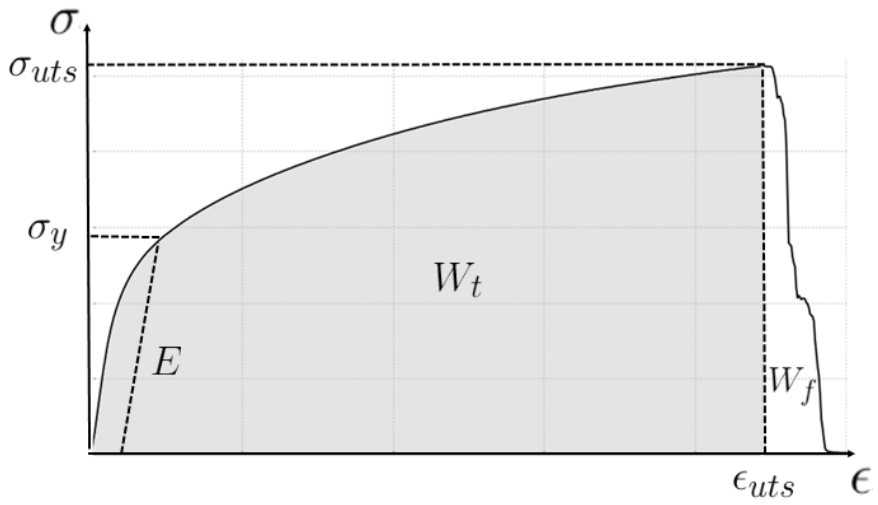

Figure 5.3: *Identification of key values.*

The results from this test will be titled Test1.

5.2 Failure and crack propagation, Test2

It turned out to be difficult to study the crack propagation and the failure characteristics in the first tensile test because of the relatively large gauge length. To make it easier to capture the crack propagation on movie and to minimize the area on which the crack is initiated, the gauge length was shortened. Therefore the same test as above was carried out again but with a gauge length of 50 mm and only in the RD, TD and 45 directions. In order to capture the crack propagation the strain rate was decreased from 9 to 5 mm/min. During this test the strain rate dependency was also studied by varying the strain rate between 2, 5 and 100 mm/min.

To be able to compare the results with the first tensile test the force displacement data from the two tests were converted into strain and stress with the relations below, where A is the cross section area (assumed unchanged during the process), L_0 is the gauge length and L is the new length of the sample. The results from this test will be titled Test2.

$$\epsilon = \frac{L}{L_0}$$
$$\sigma = \frac{F}{A}$$

5.3 Local deformation, Test3

When looking at the results from the previous tensile tests, it was realized that it would be interesting and helpful to study the deformation field on the sample during a tensile test. By doing this the lateral contraction and the strain-localization can be studied. Therefore another uni-axial tensile test was executed, this time with a DIC system. This part of this thesis was performed in cooperation with the Divison of Solid Mechanics at LTH, and their equipment was used. The tensile test was performed with a tensile stage and the DIC system consisting of two high resolution cameras and a DIC-software. The setup is illustrated in Fig. 5.4.

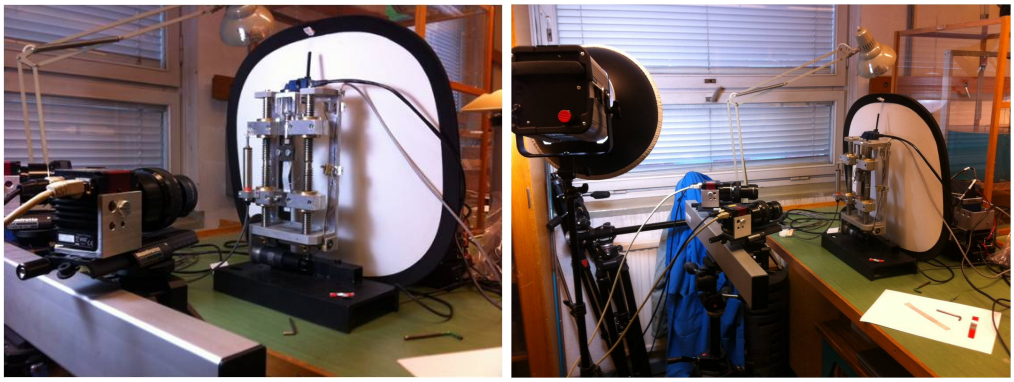

Tensile Stage *DIC system*

Figure 5.4: *DIC Setup*

The same sample proportions as in Test2 were used (gauge length 50 mm), but a speckle pattern had to be applied in order for the DIC system to work. First it was tried with only a black speckle pattern, but it turned out that the background was still too shiny. A thin white paint layer was therefore sprayed on to the samples before the black speckle pattern was applied. The speckle pattern on the sample is shown in Fig. 5.5. A strain rate of 5 mm/min was used.

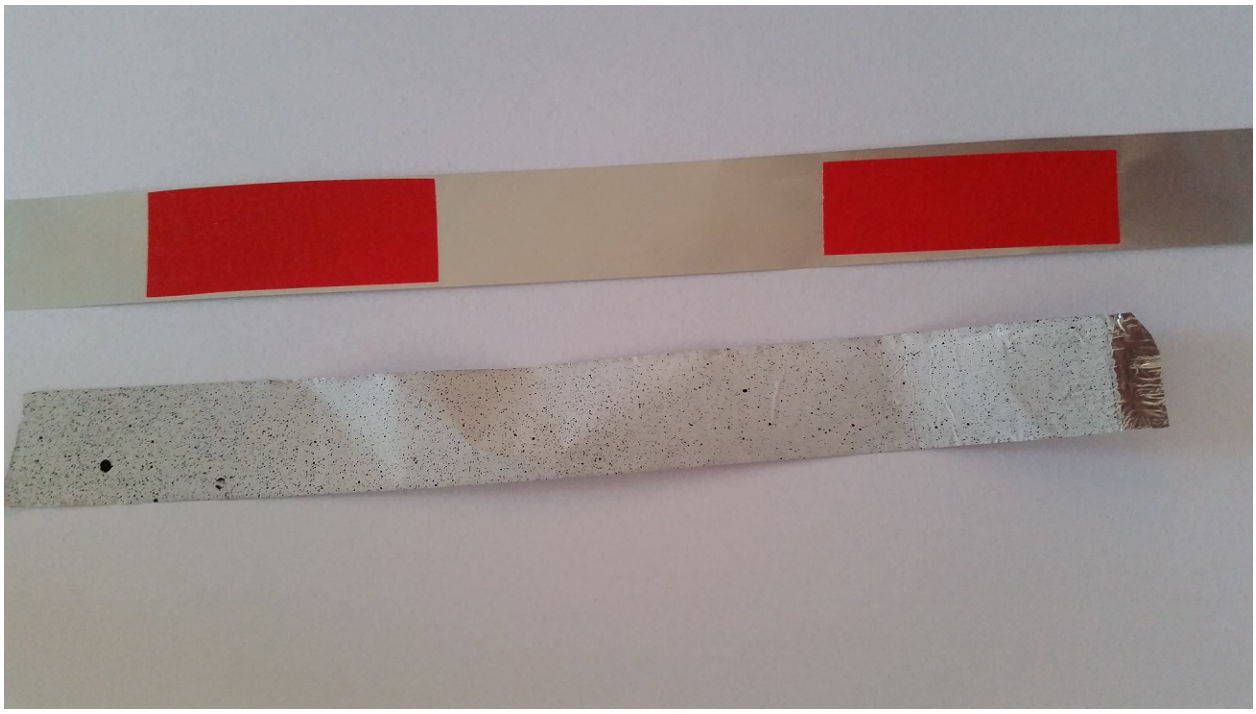

Figure 5.5: *An example of the black speckle pattern on the white background.*

The grips on the tensile stage were rough and had to be manually screwed together. It was also very difficult to align the sample in the grips since the top grip was very loose and could spin around. This will definitely affect the results. A comparison of the results from this test with the more precise uni-axial tensile test (Test2) was made in order to determine how the rough and loose grips will affect the results.

A study was also made to determine the effect paint had on the sample, this was done in the Instron machine used in the first two tensile tests since the tensile stage had too many sources of errors.

6

Results, experimental tensile tests

The results of the experimental tests are shown in this chapter. Discussion about the results will be presented in chapter 9.

6.1 Mechanical and anisotropic behaviour, Test1

Basic mechanical material characterization consists of the two principal manufacturing directions, RD and TD, complemented with the 45° direction. Results from the uni-axial tensile tests are shown in Fig. 6.1. The mean value is calculated and it becomes clear that the the deviation is very low, thus the repeatability of the test is very good. The 45° samples tend to be weaker but more ductile than the RD and TD samples. RD has a higher ultimate tensile stress, σ_{uts}, than TD but their ultimate tensile strain, ϵ_{uts}, is almost similar. The results for the remaining orientations are found in Appendix A.

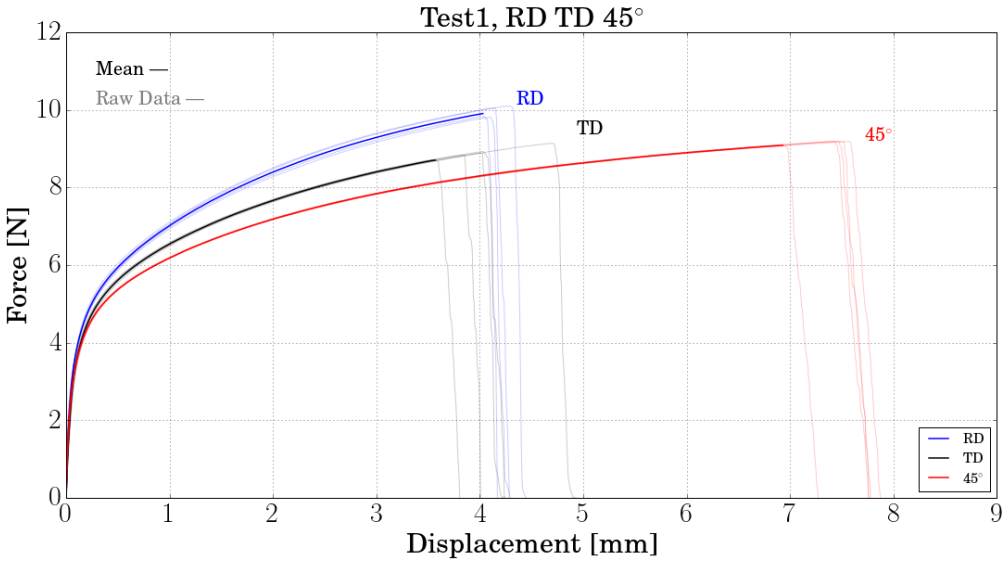

Figure 6.1: *Experimental results for directions RD, TD and 45°. Gauge length 100 mm, strain rate 9 mm/min.*

To compare all the directions the median of the results for every direction are plotted together in Fig. 6.2. The difference between the RD and 10° directions is much larger than the difference between the 40° and 50° directions. This will be discussed in chapter 9.

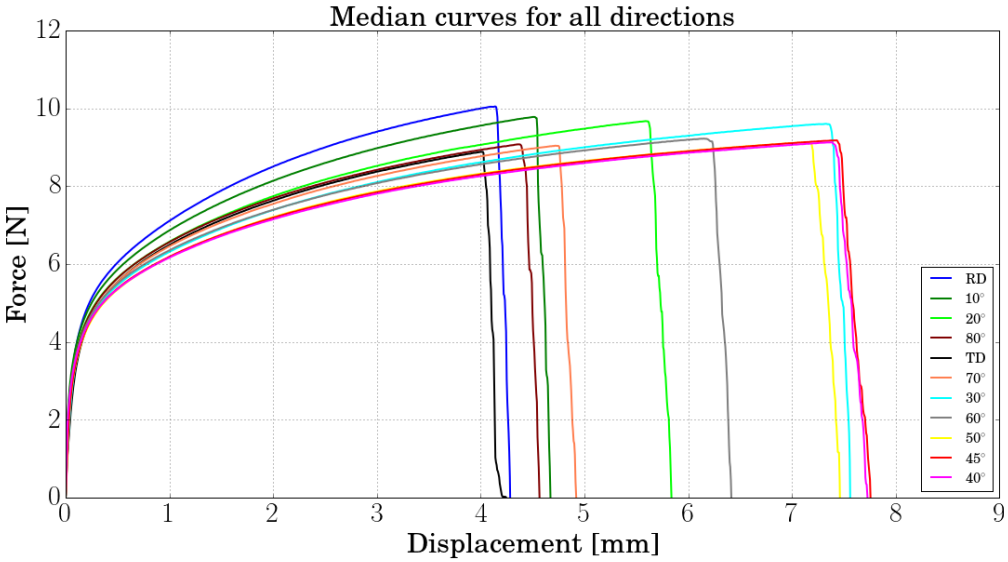

Figure 6.2: *Median curves for all directions. Gauge length 100 mm, strain rate 9 mm/min.*

Key-values

The key values needed for the curve fitting and calibration of the virtual model are shown in Table. 6.1.

Table 6.1: *The key-values needed for the calibration of the material model.*

Direction	angle α [°]	E [GPa]	σ_α $[MPa]$	σ_{uts} $[MPa]$	ϵ_{uts} [%]	W_t $[J/mm^3]$
RD	0	35.74 ± 5.41	40.66 ± 0.55	74.41	4.14 ± 0.09	2.55
TD	90	35.06 ± 3.50	38.23 ± 0.21	65.76	4.03 ± 0.38	2.14
45	45	32.67 ± 1.99	36.91 ± 0.30	67.96	7.36 ± 0.22	4.38

6.2 Failure and crack propagation, Test2

The results force vs displacement data acquired from the second uni-axial tensile test can be seen in Fig. 6.3. The repeatability from sample to sample is very good here as well. More bumps on the failure part of graph can be seen compared to the first test.

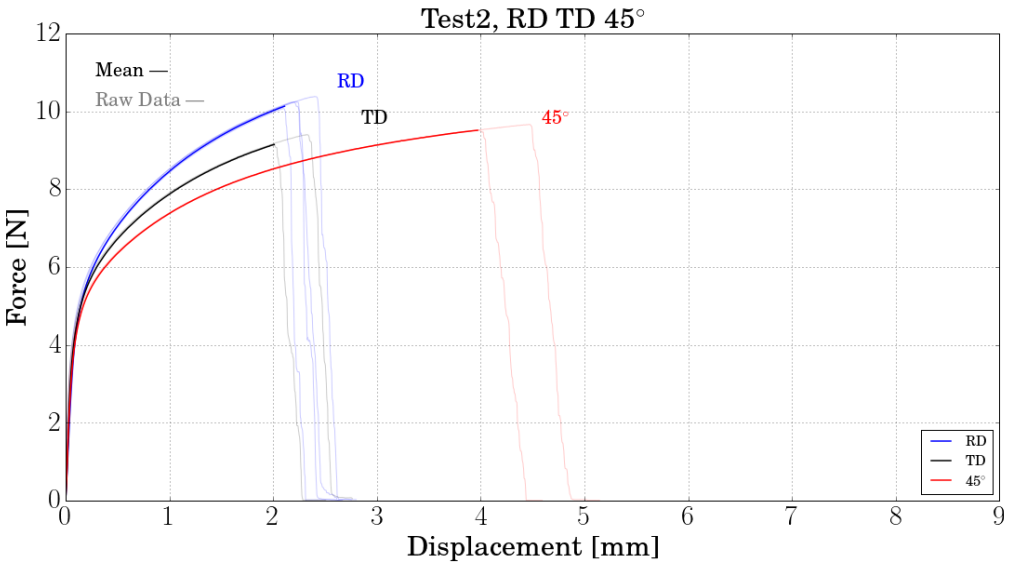

Figure 6.3: *Experimental results for directions RD, TD and 45°. Gauge length 50 mm, strain rate 2 mm/min.*

A brief study of the crack propagation was made, shown in Fig. 6.4. It can be seen that the crack follows a certain way and it reflects that in the force and displacement diagram. The strain rate was 2 mm/min and the material direction was 45°, for the Fig. below.

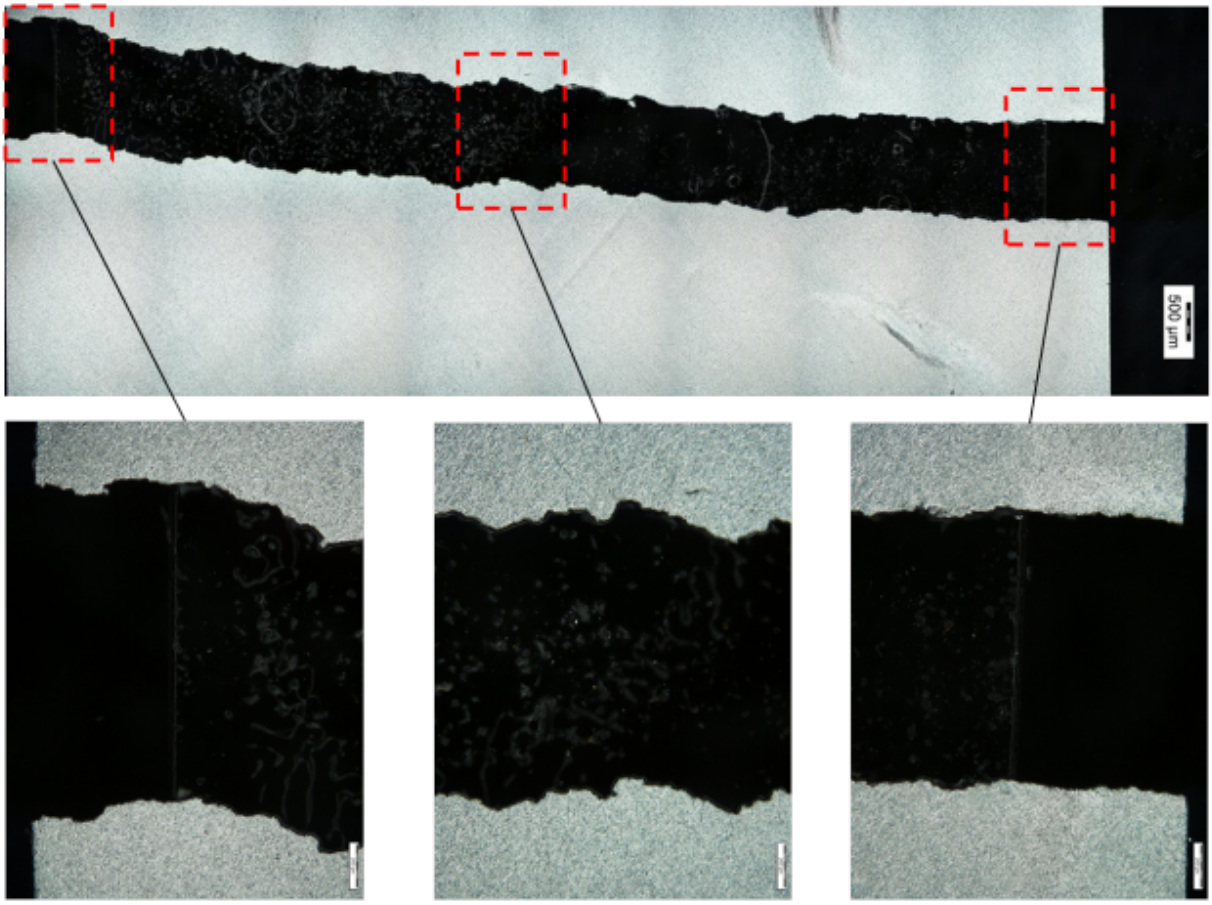

Figure 6.4: *Three different locations of the crack propagation. In this case the crack was going from left to right. The 'bumps' show that the crack changes direction. The figure at the top have the scaling 500 µm and the figures below 200 µm, [Daniela Nae, Tetra Pak].*

The strain rate was varied to determine if the results depend on the strain rate. According to the results in Fig. 6.5, this wasn't the case. The variation between the results with different strain rates are in the same order of magnitude as the variation between the results with the same strain rate.

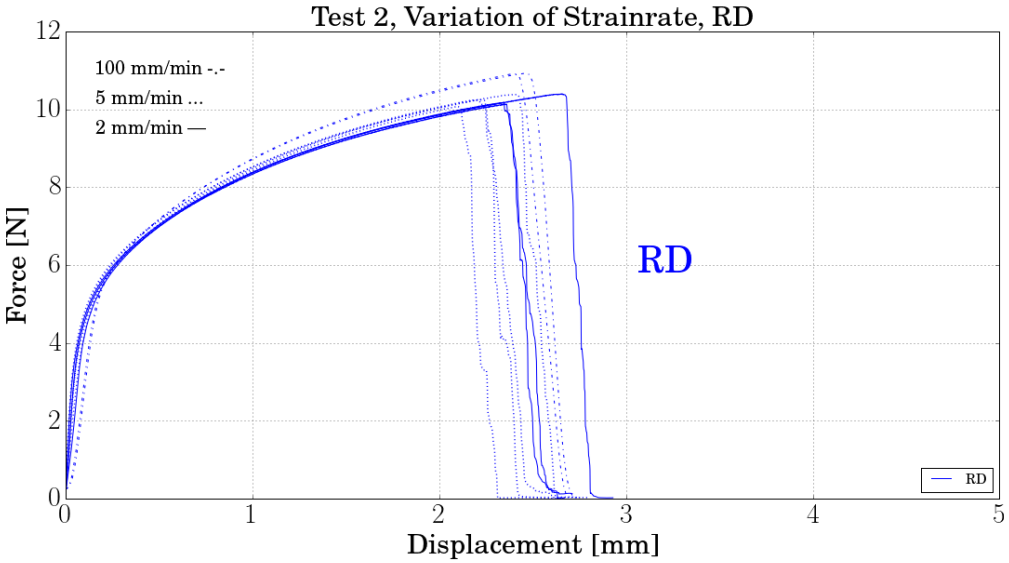

Figure 6.5: *Variation of strain rate.*

Now that it is known that the results do not depend on the strain rate, we can compare the results from Test1 (gauge length 100 mm and strain rate 9 mm/min) and Test2 (gauge length 50 mm and strain rate 2 mm/min). The samples in the second test seem to be more ductile. Besides the increase in ductility the reproducibility of the tensile test is very good. More of this will be discussed in chapter 9.

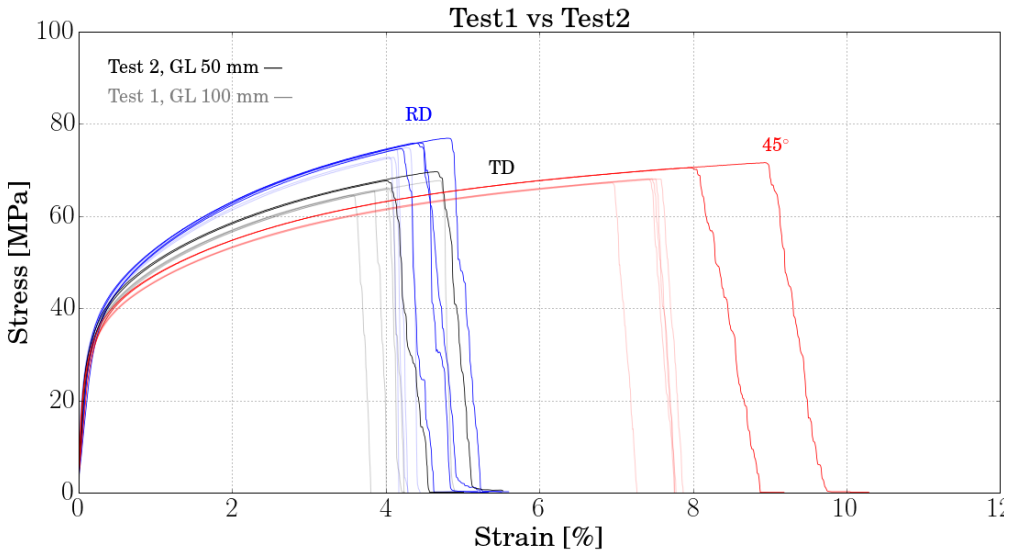

Figure 6.6: *A comparison between the two tensile tests with different gauge lengths and strain rates.*

6.3 Local deformation, Test3

Results acquired from the tensile test with the digital image correlation are colorful strain fields for every time step during the tensile test. To illustrate the strain localization we chose to show three moments in time, these are shown in Fig. 6.7. The tensile stage was connected to a computer with a software that generated force vs displacement data.

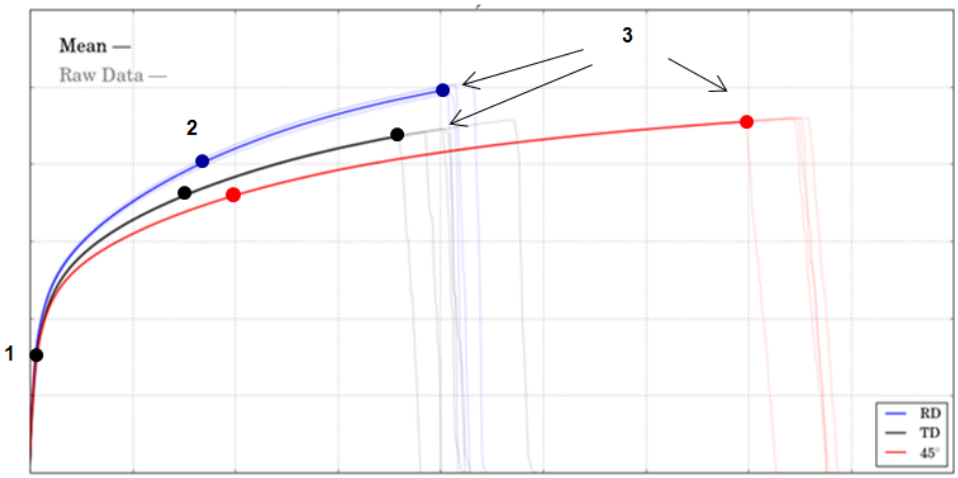

Figure 6.7: *The DIC results shown below are taken from these points during the tensile test. 1: Elastic Region, 2: Plastic Region, 3: At Failure.*

The in-situ vertical strain fields from the 3 specific points for every direction is shown below in Fig. 6.8. The first two pictures for every material orientation shows a homogeneous deformation of the sample. Strain localization in the area where the sample is about to crack can clearly be seen, third column. It is also noted that the magnitude of strain (see legend) are twice as high in the 45 direction, as seen in earlier results. During the tensile test the strain localizes to a circular area in the lower part of the sample in the 45° direction. This circular area propagates to the edge where the crack starts, this part of the sample is clearly more deformed than other parts. This i probably due to a defect in the sample.

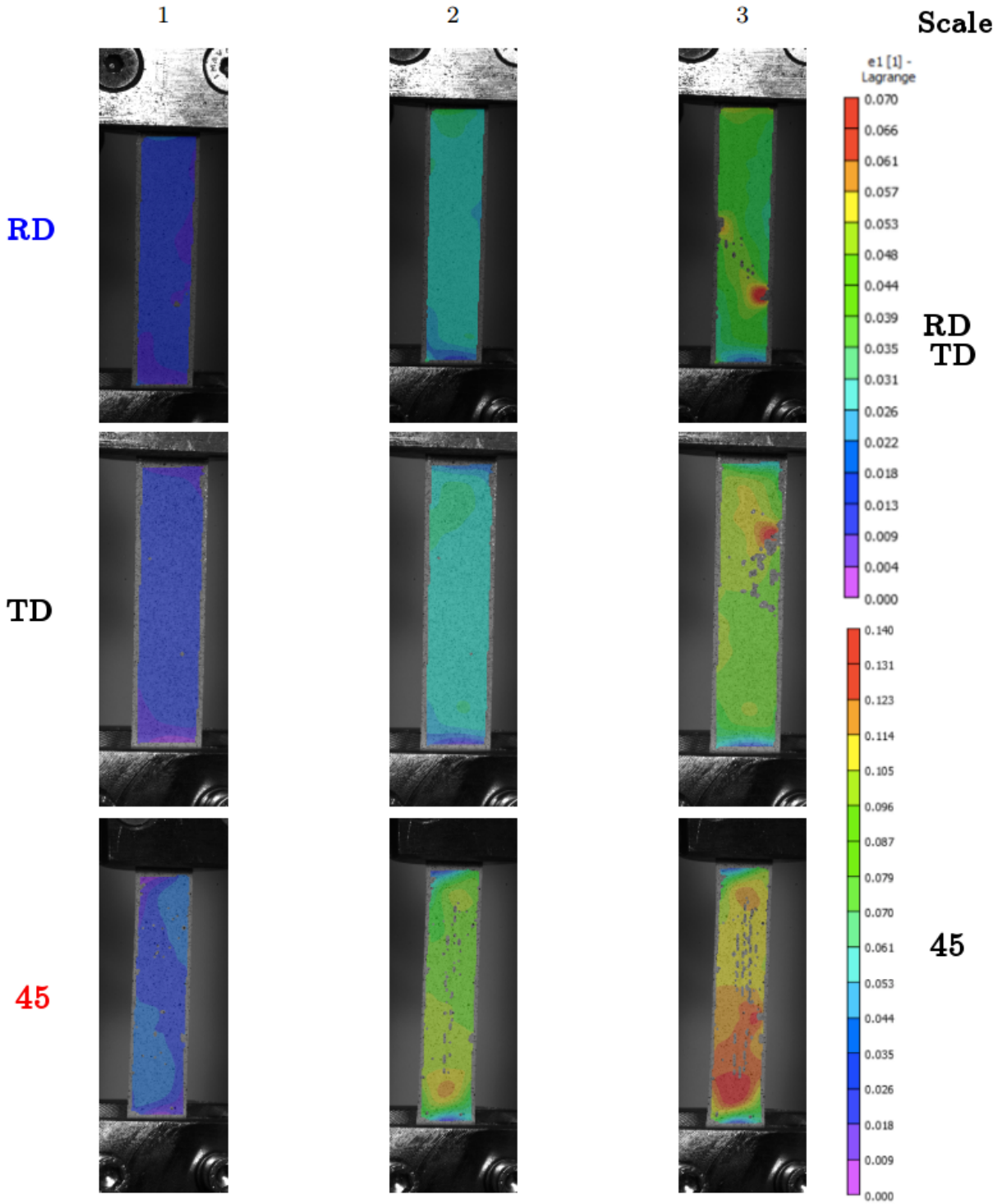

Figure 6.8: *Vertical Strain field acquired from the Digital Image Correlation system. The top row is RD, second TD and then 45. Every columns corresponds to a moment during the tensile test, shown in figure 6.7.*

The affect the grips had on the sample is shown in Fig. 6.9. It can be seen that the sample can not contract freely by the grip. When the samples were assembled it was difficult to align the grips and this can be also be seen here, the strain-field is not uniform by the grips.

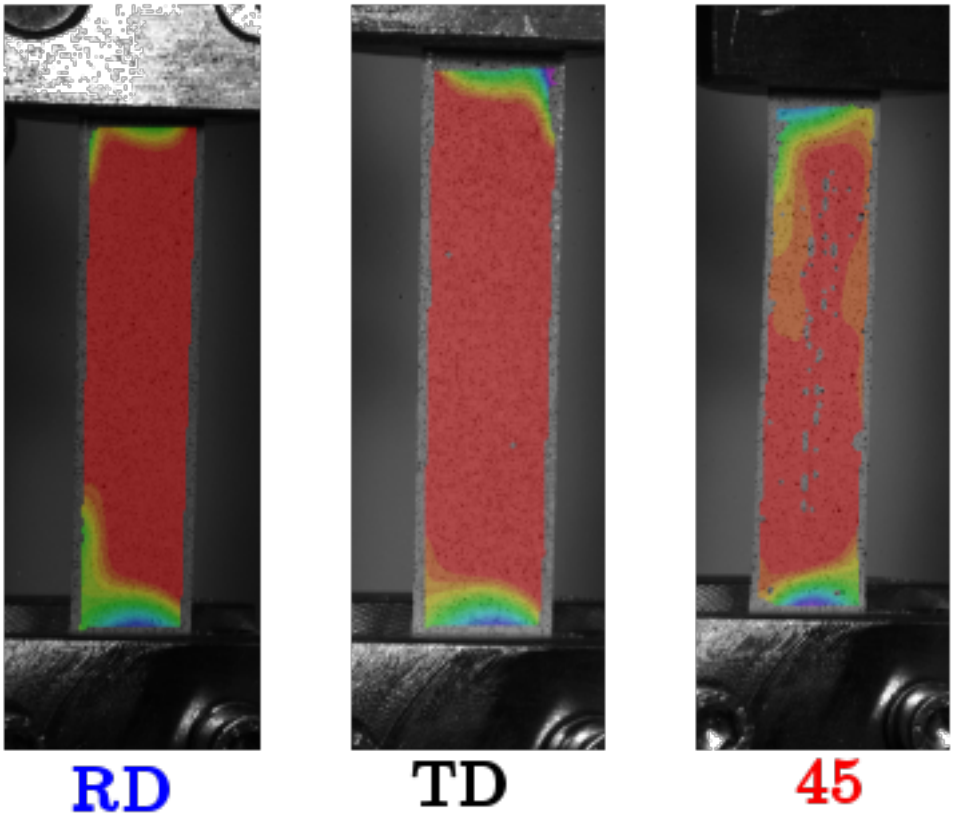

Figure 6.9: *Horizontal strain field acquired from the Digital Image Correlation system. The, in the grip, fastened part of the foil cannot contract. The images are taken from the plastic region (point 2).*

Unfortunately it was difficult to mount the aluminium foil into the tensile stage. This resulted in a large gliding effect, the sample slipped in the grips in the beginning of the test. A comparison between the more precise Instron tensile tester and the Tensile Stage at LTH is showed in Fig. 6.10. It is unclear how much the "gliding" affects the results, the magnitude of the DIC results are therefore not discussed.

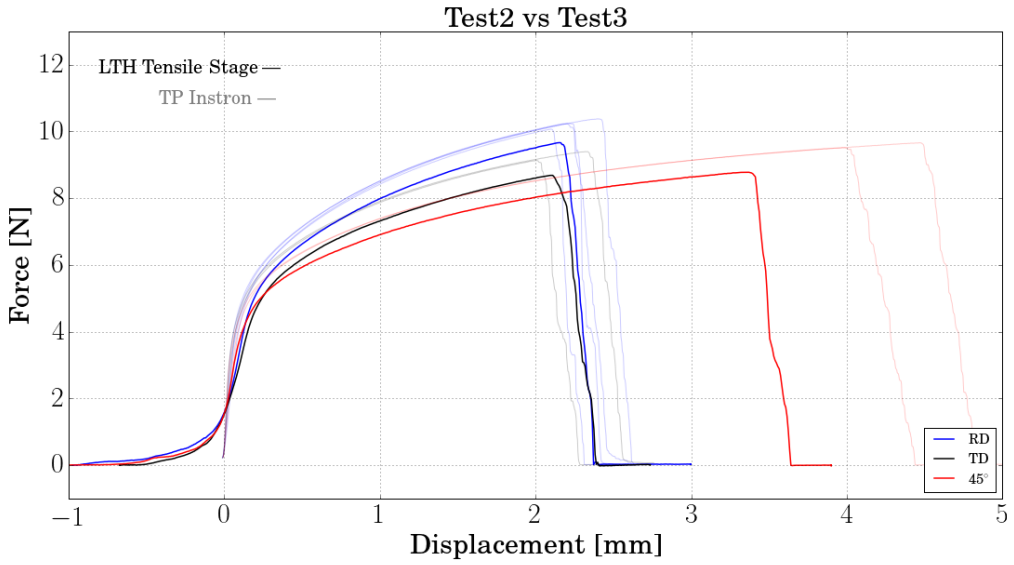

Figure 6.10: *The results from the Instron Tensile Tester compared to the Results from the tensile Stage at LTH.*

From the Fig. above it was seen that the Tensile Stage results cannot be trusted. The "effect of the paint" study was therefore executed in the Instron Tensile tester, these results are shown in Fig. 6.11. The paint does not affect the behaviour of the material (the shape of the force-displacement curve is similar) besides the strengthening effect.

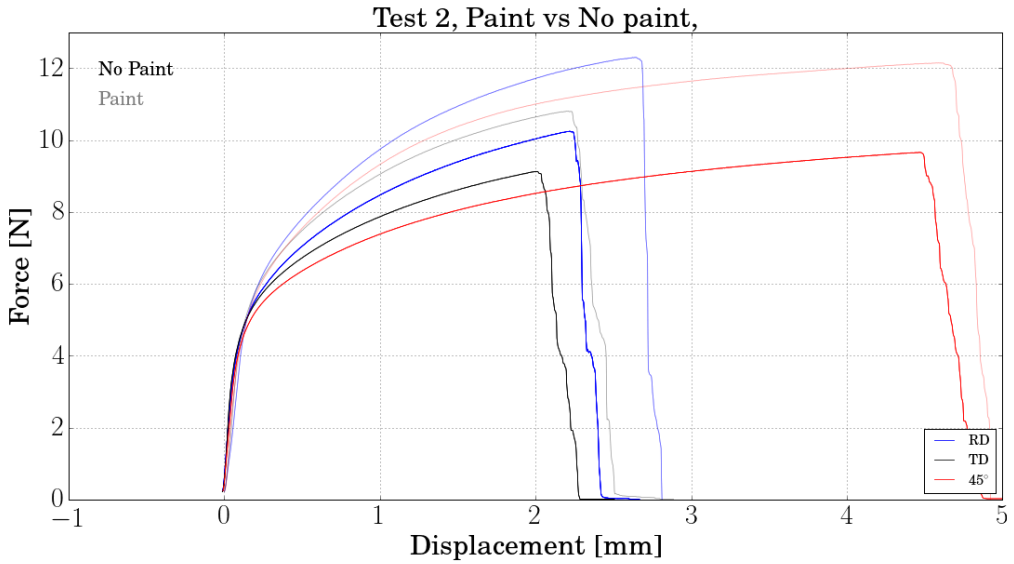

Figure 6.11: *The effect the paint had on the sample. The paint seems to strengthen the material.*

The 45° sample is showing a peculiar behaviour: it is stronger than the TD - direction. This is different from earlier results. The thickness of the paint layer was studied in order to explain this result. A micrograph of the edges of the TD and 45 ° samples is shown in Fig. 6.12.

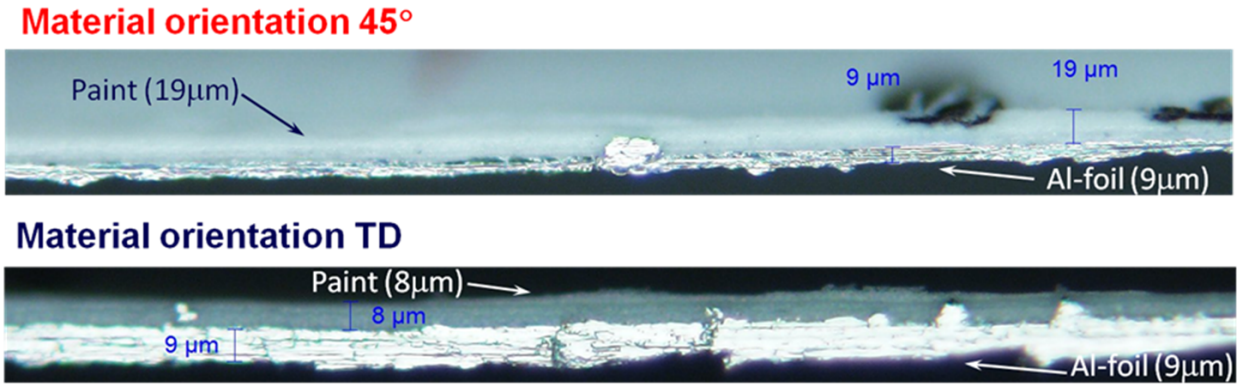

Figure 6.12: *Paint thickness, the paint layer on the 45° sample is twice as thick.*

7 Virtual tensile tests

This chapter is about simulations in order to compare the results with experimental testing later on. In this project all simulations were made in Abaqus version 6.14.

7.1 Curve fitting and calibration of material model

A parametrisation of the curve was done with an analytical model, which Petri Mäkelä has derived [Mäkelä, 2012]. Usually this model is used for paper, but it can be used for aluminium as well. This model could be calibrated with the material properties acquired from the uni-axial tensile tests. The plasticity was described with Hill's yield criterion. The curve fitting and the calibration of the model is described more thoroughly in Chapter 3.

The R-values for the Hill potential was found using the relations in Table. 3.2 and the yield stresses for the RD, TD and 45° directions from the experimental tensile tests, shown in Table. 6.1. The used R-values are showed in Table. 7.1.

Table 7.1: Normalized R-values, potential input in Abaqus.

R-values	Definition with experimental values	Calculated Value
R_{11}	$\frac{s_0}{s_0}$	1
R_{22}	$\frac{s_{90}}{s_0}$	0.923289
R_{33}	$\frac{s_{90}}{s_0}$	0.923289
R_{12}	$\frac{\sqrt{3}}{\sigma^o}\sqrt{\frac{1}{\frac{4}{s_{45}^2}-\frac{1}{s_{90}^2}}}$	0.837509
R_{13}	$\frac{\sqrt{3}}{\sigma^o}\sqrt{\frac{1}{\frac{4}{s_{45}^2}-\frac{1}{s_{90}^2}}}$	0.837509
R_{23}	$\frac{\sqrt{3}s_{90}}{s_0}$	0.90139

7.2 One element test

A good way to understand the material responses is to use one element method. The setup of this method is shown in Fig. 7.1. The setup in Abaqus is simple. The element type that was used was 3D shell element and the model was created with dimensions $3x3$ in mm, and thickness $9 \cdot 10^{-3}$ mm. The dimension was chosen after the uni-axial tensile test in order to have as little variations as possible, see next section. The boundary conditions was set as in Fig. 7.1. The solver technique can both be implicit (Abaqus/Standard) or explicit (Abaqus/Explicit), depending on what analysis that is wanted. For failure mechanics explicit is preferable and for just a tensile test simulation (without damage mechanics) implicit works well. If an implicit method is used on failure mechanics, the solution may have a hard time to converge or not even converge at all. Since failure mechanics may cause discontinuity in the solution, which may cause an inefficient solution for the implicit solution. The implicit solver technique is Newton-Raphson and this need to converge at each step and need iterations, which the explicit (forward Euler) does not need. When all settings are done the test can be started and thereafter evaluated.

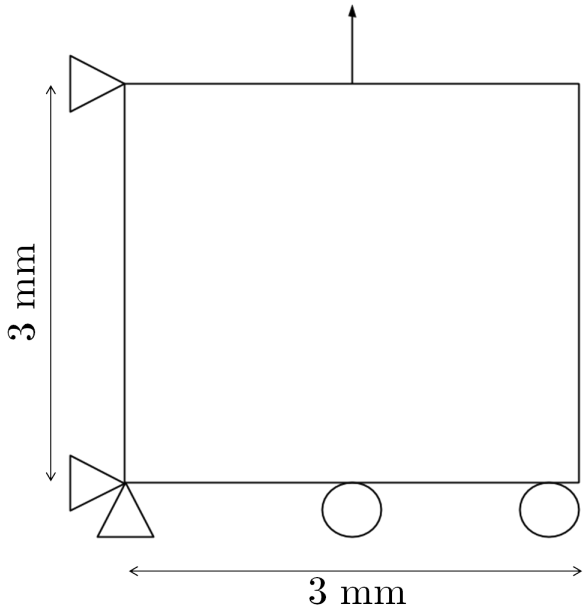

Figure 7.1: *Main setup of one element test.*

7.3 Uni-axial tensile test

The setup in this model is basically the same as for the one element test but with some small differences. Figure 7.2 shows what the model looked like. As seen in Fig. 7.2, the mesh and the model is in sample dimensions. Each mesh rectangle have about the same dimension as in the one element test, that is $3x3$ and thickness $9 \cdot 10^{-3}$ in mm. Since the sample was attached on both ends and it was only the upper attachment that moved, new boundary conditions was introduced. The new boundary conditions can be seen in Fig. 7.2. To make it less complicated, no failure mechanics was introduced. To match the experimental tensile tests the displacement was chosen to 9 mm. An implicit solver technique was chosen. The material orientation could be changed under the *Part*-section in Abaqus in order to match every direction.

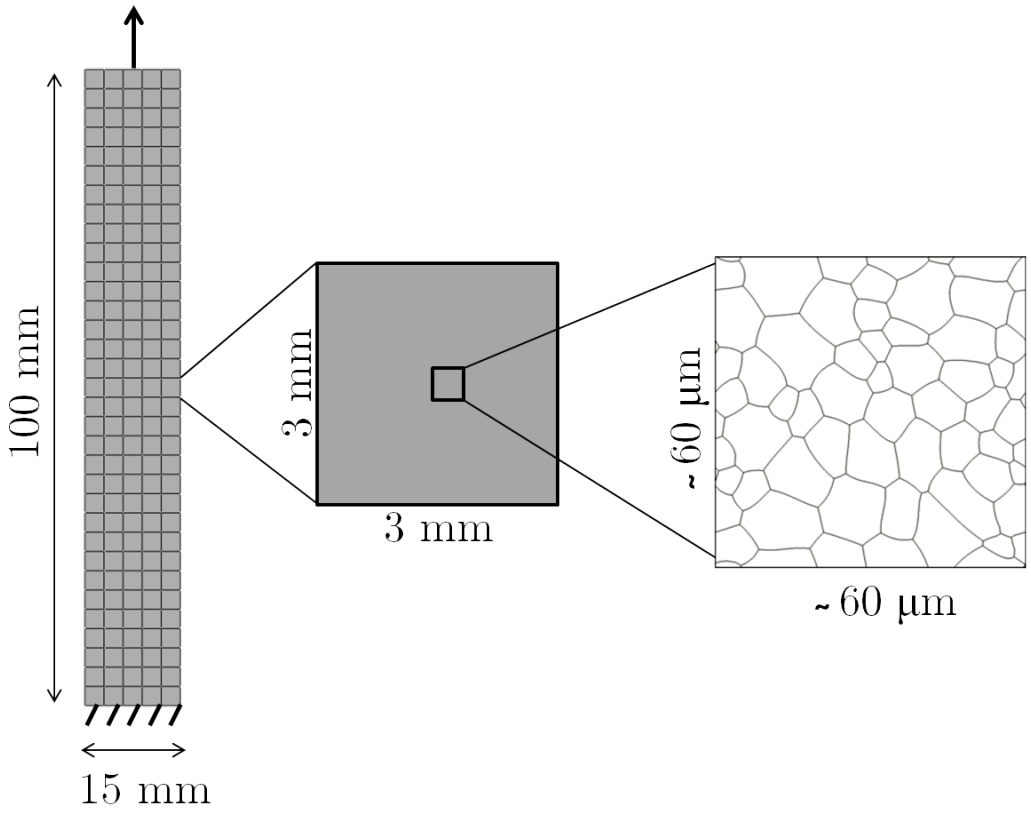

Figure 7.2: *Main setup of the virtual tensile element test. To the left is the actual mesh in Abaqus. To the right is one element from the mesh showing that it fits many grains.*

7.4 Damage mechanics

With the same setup as in *Uniaxial tensile test*, it is possible to introduce failure criteria. This is done under the *material*-section in Abaqus. In this project two criteria were used, FLD and FLSD. It was only one point that was used and the major option was set to 0.08 and minor 0 for FLD. In a similar way for FLSD, major was set to 76 MPa and minor 0 MPa. Both these major options were chosen after the result of the first tensile test (Test1) in order to match the simulation, see Fig. 6.1. Both criteria need damage evolution, and the chosen type was energy with linear softening. The damage evolution is needed to describe the post damage-initiation material behaviour. What it describes is the rate of degradation of the material stiffness. The degradation was multiplicative and the failure energy was chosen to 1. All these parameters were picked to fit the simulation as good as possible.

8 Results, virtual vs experimental tests

The results in this chapter will show the connection of the virtual tests with the experimental.

8.1 Uniaxial tensile test

Curve fitting

How well the analytical curve fits the experimental results are shown in Fig. 8.1. Ramberg-Osgood analytical expression seems to fit very well but differs most in the elastic region, shown in Fig. 8.2.

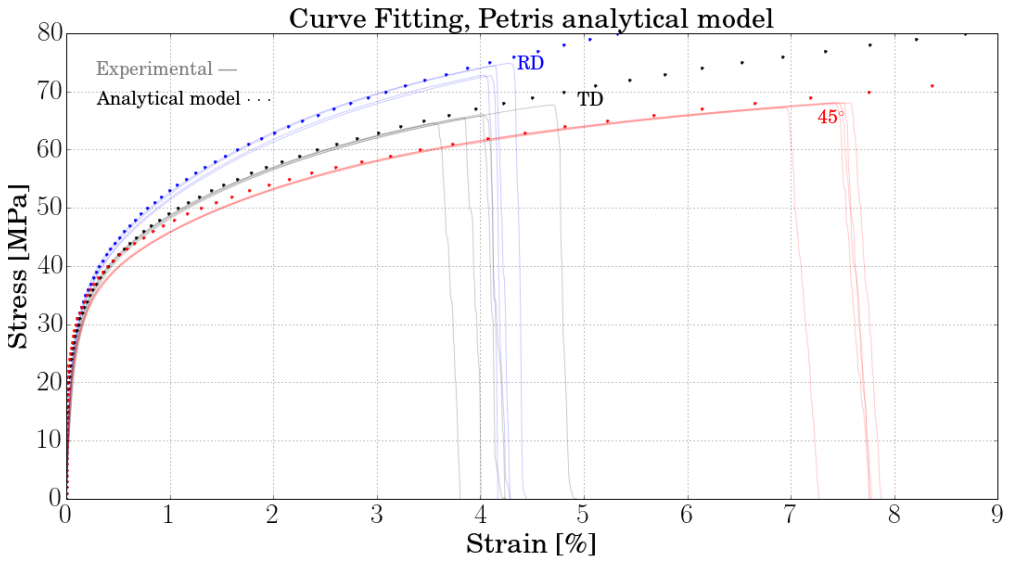

Figure 8.1: *Analytical approach.*

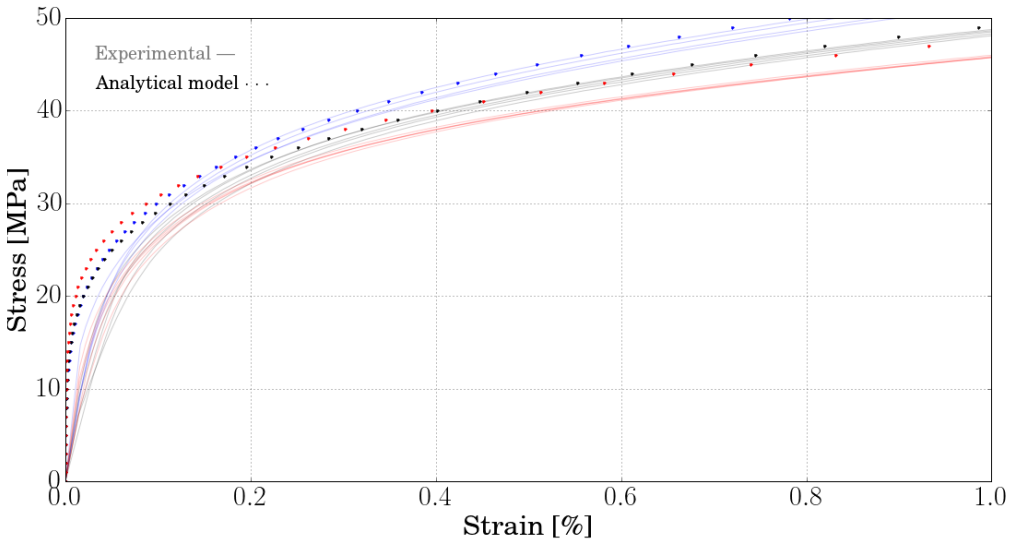

Figure 8.2: *Zoomed in with focus on the elastic region.*

Calibration and yield criteria

One part of the project was to identify the mechanical behaviour including the anisotropy of the material, and fit this into a yield surface which is shown in Fig. 8.3. The solid curve show a typical isotropic yield surface where the intersection with the two axes occur at the same magnitude. However, for the dashed curve it can be seen that it does not intersect at the same magnitude on the two different principal stress axes.

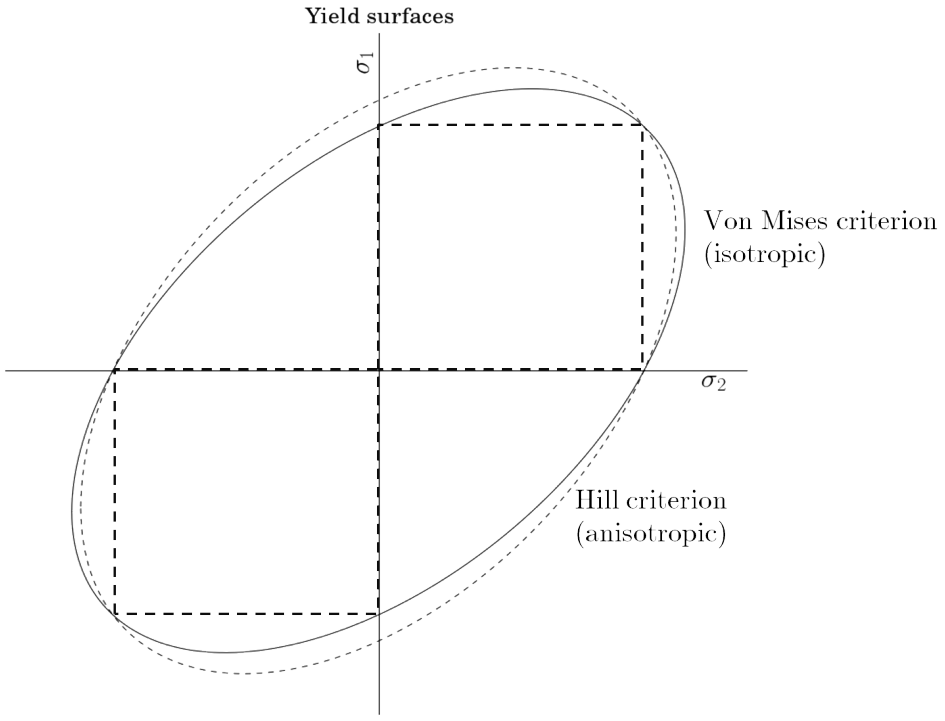

Figure 8.3: *von Mises yield surface (thick line) and Hill's yield surface (dashed line), showing the anisotropy of the material.*

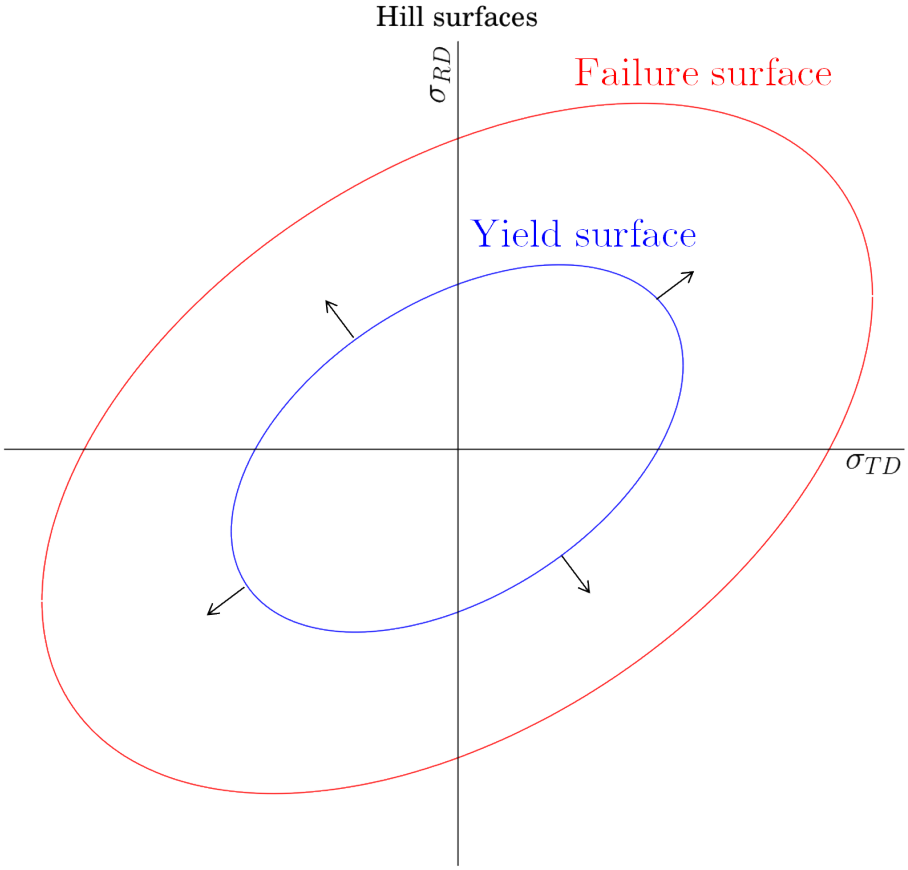

Figure 8.4: *Hill surfaces for yielding and for failure. The black arrows indicates how the evolution of the surface occur.*

Figure 8.4 show an isotropic hardening, i.e. the size changes but the position and shape remain the same. How well the calibrated model fits is shown in Fig. 8.5. The model intersect with RD, TD and 45° since these were the calibration angles. With the remaining angles it can be seen that the angles between RD and 45° are overestimated. The angles between 45° and TD are underestimated.

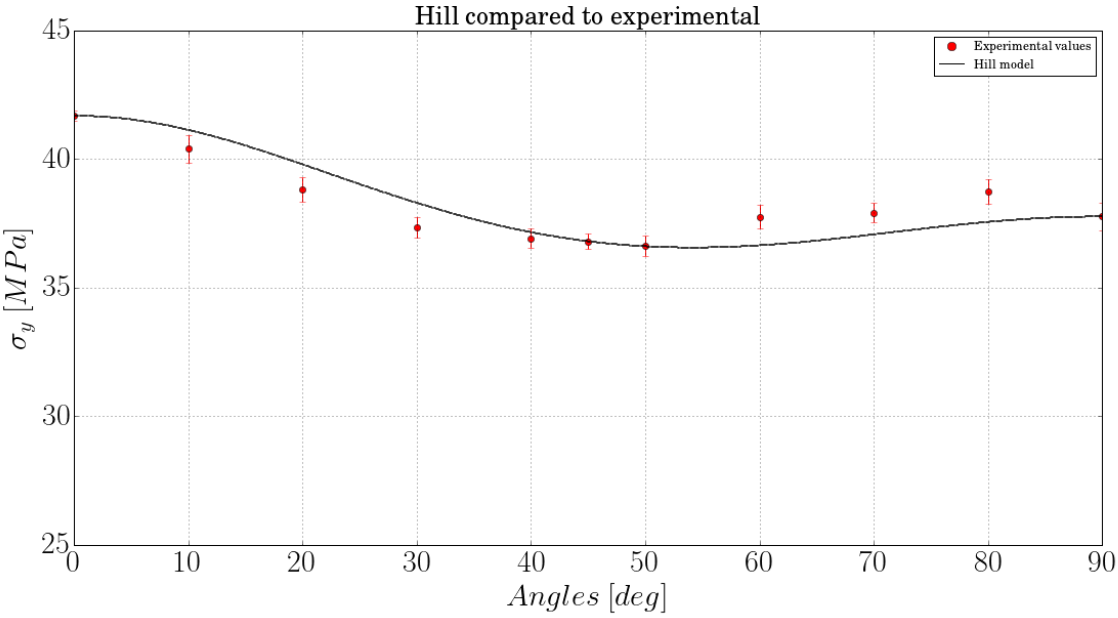

Figure 8.5: *The calibrated Hill model compared to the experimental data, the standard deviation for the experimental results are shown as bars.*

The response of the material model is shown in Fig. 8.6. Where Fig. 8.6a show how well the calibrated model fits with the experimental results. How the virtual model fits the experimental results from the remaining orientations can be found in Appendix A. The deviation is quantified with the coefficient of determination, namely the R^2-value, Eq. (8.1) where M is the measured values, S is the simulated values and S* is the mean of the simulated values.

$$\begin{aligned} R^2 &= 1 - \frac{SS_{err}}{SS_{tot}} \\ SS_{err} &= \sum_i (S_i - S^*)^2 \\ SS_{tot} &= \sum_i (M_i - S^*)^2 \end{aligned} \tag{8.1}$$

Figure 8.6b is the same as Fig. 8.6a but zoomed more on the elastic region, in order to see what happens during this part.

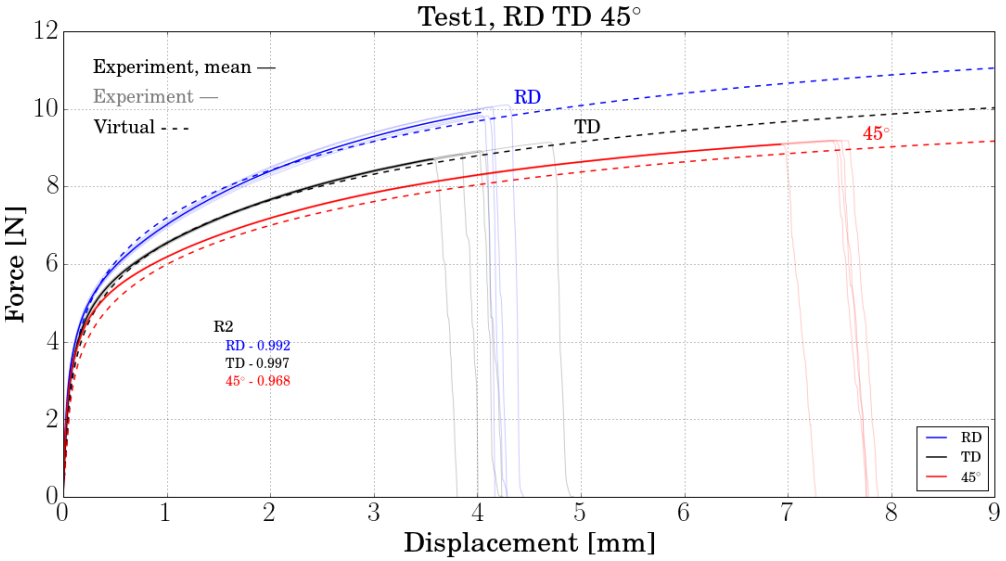

(a) *The full figure with R^2-values*

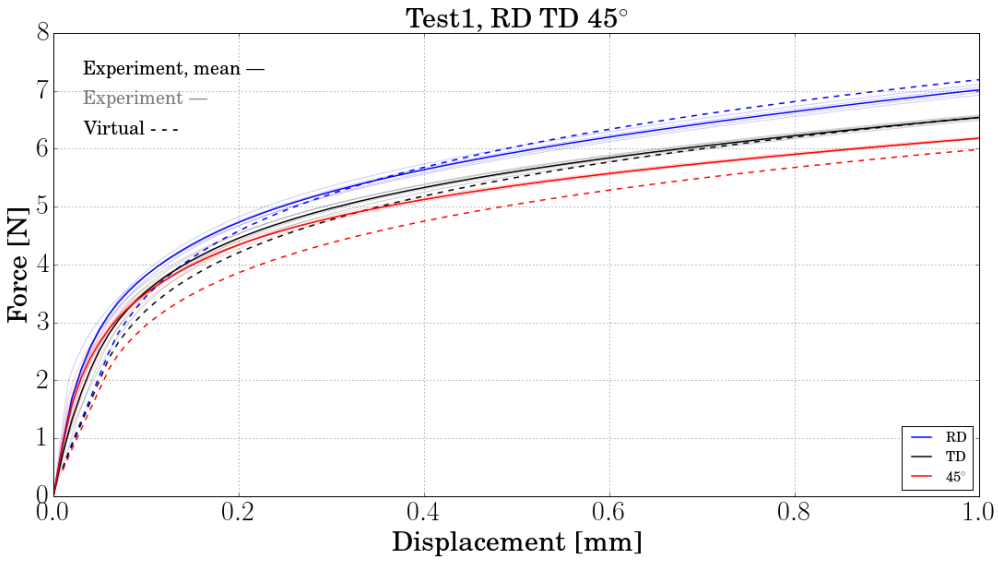

(b) *Zoomed figure with more focus on elastic region*

Figure 8.6: *Virtual tensile test vs experimental tensile test for directions: RD, TD and 45°.*

8.2 Uniaxial tensile test with damage mechanics

Simulated damage mechanics can be seen in Fig. 8.7. Both FLD and FLSD were used, and it can be seen that RD and 45° fits well. However, TD does not fit that well and this will be discussed in chapter 9.

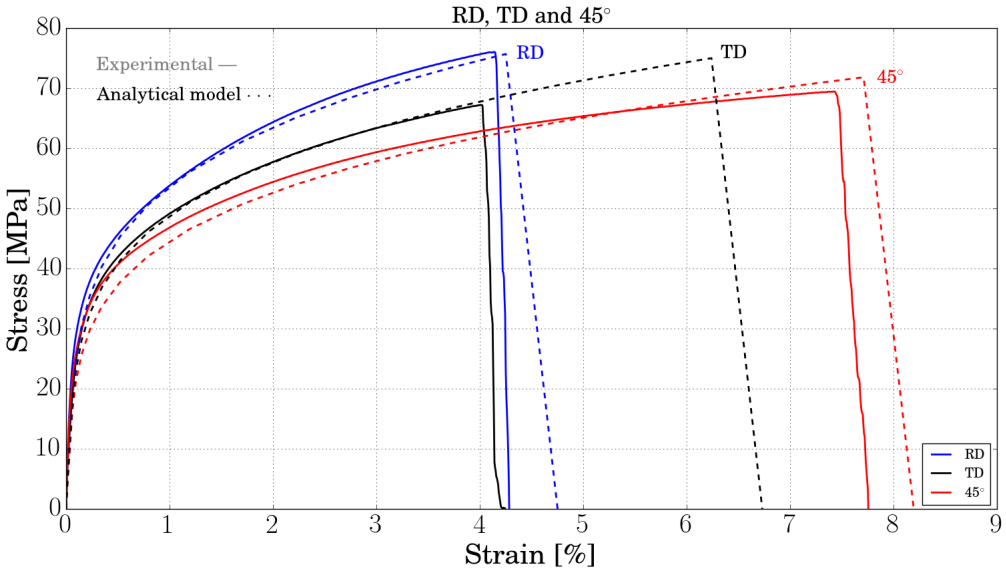

Figure 8.7: *Simulated damage mechanics for the RD, TD and 45° directions.*

9 Discussion

9.1 Results of the tests

This project have many parts and therefore the discussion will be divided according to the corresponding test.

Test1, mechanical and anisotropic behaviour

In this test an advanced characterization of aluminium-foil was performed. The results clearly show that the material has anisotropic characteristics, shown in Fig. 6.2. The repeatability of the test is very good and the standard deviation is low for all directions, as seen in Table. 6.1. The orientation with the largest standard deviation is RD. This is probably due to the sample preparation. An angle difference was more difficult to spot with the bare eye in the RD direction than in for example the 45. Thus there is a larger chance that the some of the cut out RD samples have an orientation of a couple of degrees larger or smaller than 0 degrees. Figure 6.2 shows that the directions from 45° to TD basically have the same σ_{uts}, but for RD to 45° it varies. This may imply that the directions from RD to 45° are a bit more sensitive when it comes to σ_{uts}.

Figure 6.1 shows that there are some differences when the samples break, i.e. ϵ_{uts} vary for every orientation. This is probably connected to the edge defects, from the cutting, on the samples. Edge defects may weaken the material at a specific location. When the material is under loading, this point weakens faster and eventually causing the material to fail. To avoid edge defects a bulge test can be performed.

As mentioned before, ϵ_{uts} is almost twice as large for the 45 direction as for RD and TD. The reason for this has been thoroughly discussed during this project and to answer this a study of the behaviour of the microstructure during load deformation has to be made. There seems to be a connection between the amount of shear stress triggered in the material and the yield stress and elongation. This was not the main focus of this thesis but a main conclusion in this area can still be made: The characteristics in the micro scale is the main factor for the difference between the orientation in both yield stress and the elongation between the different orientations.

Test2, failure and crack propagation

The comparison between the two tests with different Gauge length can be seen in Fig. 6.6. Even though the test was made several weeks after one another and with different gauge length, the difference between the results are small. It can therefore be concluded that the test method used is both repeatable and reproducable. When comparing the tests one needs to bare in mind that the reduction in gauge length triggers two sources of error: ratio between edge defects and sample size is smaller and the tensile energy per area is larger. Both of these can be the reason for why the elongation in Test 2 is larger for all the

orientations. But as discussed earlier the point for failure is mainly due to edge defect and to further study the failure behaviour a bulge test is needed.

During crack propagation the crack changes direction and the feedback of that can be seen in Fig. 6.6. Especially when looking at the curves for gauge length 50 mm in 45°. The 'bumps' in the curve (the failure part of the curve) is when the crack changes direction and Fig. 6.4 clearly show that the crack changes direction during failure.

Test3, local deformation

The DIC results was a long shot in this thesis, applying paint on micrometer thick aluminium foil seemed in the beginning hopeless, but it turned out that it was actually not that problematic. As long as a reference test is done without paint the effect of the paint can be quantified and the data from the test can be adjusted accordingly. Unfortunately the tensile stage used in the DIC test contributed to many sources of errors and this turned out to be the main problem during this test, and not the paint as expected. Still, the acquired strain fields show a homogeneous deformation before failure and a localization of strain in the crack surroundings.

In the strain field from the 45 direction, shown in Fig. 6.8, it can be seen that the material starts to weaken from the middle of the sample and out to the crack. The strains will always localize where the material is the weakest. From that image one could expect that the crack would initiate in the middle of the sample, however this is not the case. When the material in the middle deforms, it deforms plastically, which strengthens the material. The strains will localize to the next weak area and so forth until the crack initiates.

As mentioned it was problematic to mount the sample into the tensile stage, which contributed to a misalignment of the sample. The strain field in 6.8 shows proof of this, the uni-axial loading triggers shear in the material since the lower and upper grips are not aligned. Very interesting results can be acquired from a DIC test, but in order to actually be able to use the results the sources of errors need to be minimized. Therefore it is suggested that another DIC test is made but with a tensile test in an Instron machine, equipped for testing on aluminium foil, that produces more trustworthy results.

Virtual compared to experimental

The chosen analytical approach was Ramberg-Osgood, according to Eq. (3.3). This was calibrated after the experimental results and fits well, shown in Fig. 8.1. The part that have most differences is the elastic region, shown in Fig. 8.2. This variation depends on how the Young's modulus was calculated. Also, Young's modulus was calculated in different programs by different persons, implying that this is also a source of error. Overall, the analytical approach fits well. The feedback from the tensile simulation in Abaqus is shown in Fig. 8.6. Fig. 8.6a shows R^2-values, which are above 0.95. That the R^2-value is high means that the model is good, even though it uses a rough mesh. To put this in perspective, an average grain size is about 10 μm in diameter and the used element size is 3x3 mm. This means that each element can fit a lot of grains (about 100 000 grains in these measurements), which Fig. 7.2 implies.

As mentioned before, the material is anisotropic and Fig. 8.3 shows this. The black curve is the isotropic case (von Mises), and to show this there are two squares with the same size. The squares show the intersection with each axis, implying that the intersection have the same magnitude. But the other curve (the blue) show an anisotropic case, i.e. the intersection does not have the same magnitude on the different axes. This blue curve is Hill orthotropic yield criterion and to achieve this some assumptions had to be made. First of all plane stress was assumed, then that the material is orthotropic and last transverse isotropy ($s_{22} = s_{33}$). Of course this simplified the model, but even with these simplification the model fits well, which Fig. 8.5 shows. The black line (Hill model) intersects with the experimental values (red dots) for RD, TD and 45°. This is not surprising since these directions were the calibration directions. A study of the evolution was also made, shown in Fig. 8.4. What can be seen in Fig. 8.4 is that isotropic hardening occurs, that is that the position and shape remains the same but the size changes of the yield surface. Note that the anisotropy is not high since the blue curve doesn't differ much from the black in Fig. 8.3.

A brief study on the damage mechanics was also made in the virtual testing, shown in Fig. 8.7. This figure shows that with only two criteria, which were simplified, the damage mechanics could be captured. Since only one point was used in each criterion there are some shortcomings. With the minor option set to 0 the criteria are independent of material direction, and thus the breaking value (major option) was fit after RD (for FLSD) and 45° (for FLD). Figure 8.7 shows that RD and 45° fits well, but TD does not fit at all. Applying this with all material directions would lead to some inaccuracy.

9.2 Concluding remarks

This thesis can be concluded with the following remarks.

- Aluminium is clearly anisotropic.
- The calibrated material model reflects the anisotropic behaviour of aluminium foil very well.
- The mechanical behaviour of aluminium foil is crucially dependent on the microstructure.
- Damage mechanics is associated with microstructure but can be modeled at a macroscopic length scale.
- The simple modeling approach is applicable on foils from other suppliers

9.3 Further work

Validate with bulge test As mentioned in the discussion a bulge test could not only validate the results but also help to get a better understanding of the "actual" failure behaviour, not triggered by edge defects.

Validate with different foil The material model in this thesis is from the beginning meant to be used on paper material, but in this thesis it has been calibrated for aluminium foil. To validate that the calibration process can be repeated for all types of foils more tests need to be made.

Damage mechanics: XFEM XFEM is a technique evolved from the Finite Element Method. To simulate failure in FEM the elements through which the crack propagates are deleted and the propagation is highly dependent on the mesh type. In order to better reflect the crack propagation XFEM separates and splits elements instead of deleting them, by doing this the curvature of the crack can better be simulated and the physical behaviour can be better captured.

Damage mechanics: optimize failure criteria For this thesis the damage mechanics have been simulated as if it were independent of material direction. Instead of using one point in the criteria it would be preferable to use one of them (FLD or FLSD) using both major and minor values. This could capture the anisotropy for the damage mechanics. It is also worth mentioning that more criteria can be evaluated.

DIC Poisson's ratio In this thesis is has been assumed that Poisson's ratio is constant during uni-axial load but this might not be the case. With DIC the contraction in width (in plane) and thickness (out of plane) can be captured, from this the Poisson's ratio can be determined. The DIC results from this thesis had to many sources of error to actually come to any conclusions. A further investigation of the effect of the paint and an optimization of the speckle pattern would definitely result in more usable data.

Microstructure behaviour during loading This would indeed be very interesting to further study. A tensile test of the aluminium foil under a microscope and/or with TEM (Transmission Electron Microscopy) could explain how the microstructure actually affects the mechanical characteristics.

Bibliography

[Abaqus, 2015] Abaqus, v. . (2015). Abaqus manual 2015. http://www.egr.msu.edu/software/abaqus/Documentation/docs/v6.7/books/usb/default.htm?startat=pt05ch18s02abm20.html.

[Callister, 2001] Callister, J. W. D. (2001). *Fundamentals of Materials Science and Engineering*.

[Hallberg, 2013] Hallberg, H. (2013). A modified level set approach to 2D modeling of dynamic recrystallization. *Modelling and Simulation in Materials Science and Engineering*, 21(8):085012.

[Hallberg and Ristinmaa, 2013] Hallberg, H. k. and Ristinmaa, M. (2013). Microstructure evolution influenced by dislocation density gradients modeled in a reaction-diffusion system. *Computational Materials Science*, 67:373–383.

[Hill, 1948] Hill, R. (1948). A theory of the yielding and plastic flow of anisotropic metals. 193(1033):281–297.

[LaVision, 2010] LaVision, F. o. i. (2010). Digital image correlation. http://www.lavision.de/en/techniques/digital-image-correlation.php.

[Level and Federation, 1994] Level, B. and Federation, A. (1994). The Rolling of Aluminium : the Process and the Product 1301 The Rolling of Aluminium : the Process and the Product.

[Mäkelä, 2012] Mäkelä, P. (2012). An analytic procedure for determination of fracture toughness of paper materials. *Nordic Pulp and Paper Research Journal*, 27:352–360.

[Mäkelä and Östlund, 2003] Mäkelä, P. and Östlund, S. (2003). Orthotropic elastic-plastic material model for paper materials. *International Journal of Solids and Structures*, 40(21):5599–5620.

[Ramberg and Osgood, 1943] Ramberg, W. and Osgood, W. R. (1943). Description of stress-strain curves by three parameters.

[Schreier et al., 2009] Schreier, H., Orteu, J.-J., and Sutton, M. a. (2009). Frontpage. *Image Correlation for Shape, Motion and Deformation Measurements. Basic Concepts, Theory and Applications*, pages ii–xx.

[Stawovy et al., 2000] Stawovy, M. T., Aning, A. O., Kampe, S. L., Reynolds, W. T., and Wert, J. a. (2000). Processing of Aluminum Alloys Containing Displacement Reaction Products Processing of Aluminum Alloys Containing Displacement Reaction Products.

[Total Materia, 2015] Total Materia, T. w. m. c. m. d. (2015). Aluminum grades. http://www.totalmateria.com/page.aspx?ID=AluminumGrades&LN=EN.

A

Results for the remaining orientations

A.1 Experimental Results

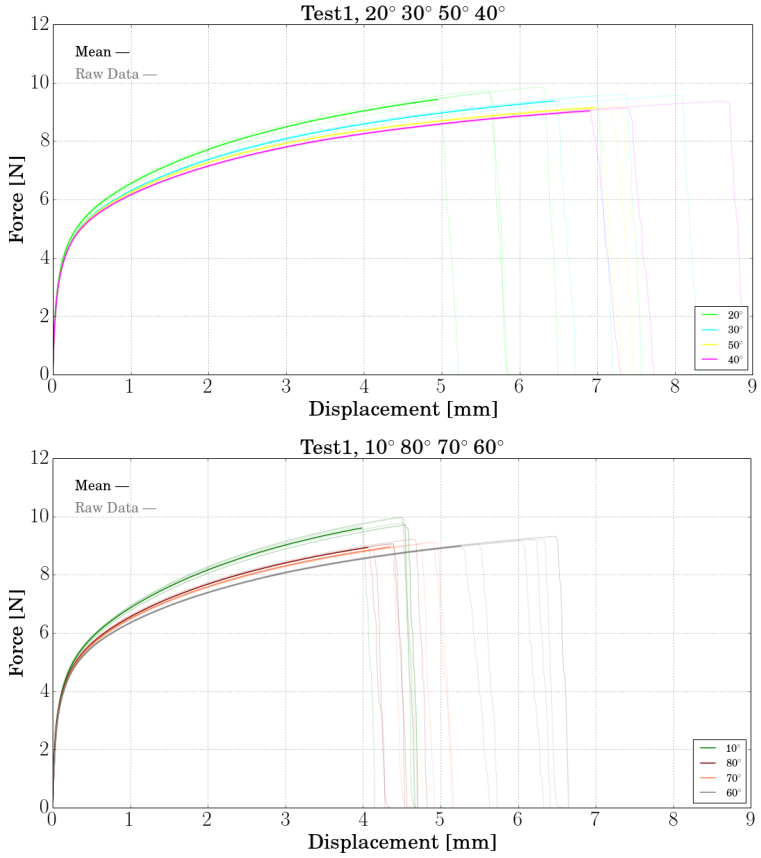

Figure A.1: *Experimental results for the remaining orientations*

A.2 Key-values

Table A.1: Key-values

angle α [°]	E [GPa]	σ_α $[MPa]$	σ_{uts} $[MPa]$	ϵ_{uts} [%]	W_t $[J/mm^3]$
0	35.74 ± 5.41	40.66 ± 0.55	74.41	4.14 ± 0.09	2.55
10	34.00 ± 3.77	39.86 ± 0.48	72.41	4.42 ± 0.21	2.73
20	30.43 ± 0.89	38.94 ± 0.38	71.62	5.59 ± 0.46	3.39
30	32.79 ± 3.27	37.33 ± 0.45	71.11	7.18 ± 0.59	4.45
40	30.05 ± 2.25	37.11 ± 0.40	67.59	7.63 ± 0.72	4.34
45	32.67 ± 1.99	36.91 ± 0.30	67.96	7.36 ± 0.22	4.38
50	33.07 ± 0.78	37.02 ± 0.38	67.63	7.12 ± 0.15	4.21
60	36.12 ± 2.92	37.32 ± 0.49	68.30	6.03 ± 0.45	3.63
70	36.44 ± 3.40	37.92 ± 0.47	66.94	4.67 ± 0.22	2.68
80	35.25 ± 3.77	38.40 ± 0.54	67.21	4.32 ± 0.21	2.50
90	35.06 ± 3.50	38.23 ± 0.21	65.76	4.03 ± 0.38	2.14

A.3 Experimental vs virtual Results

The experimental vs virtual results for all the remaning orientations.

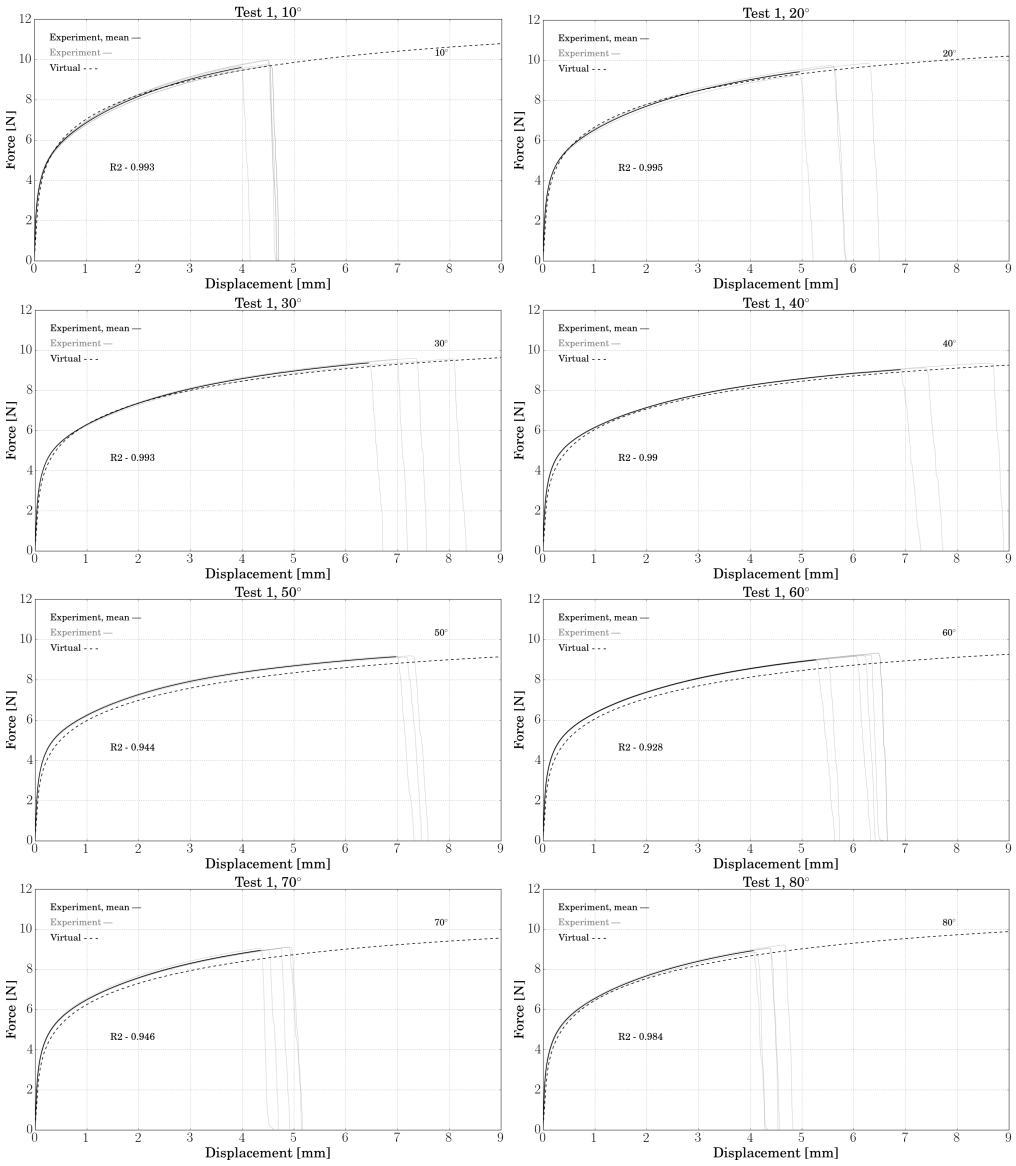

B

Transformation of stress

A simple 2D scenario can be divided into the stresses shown in Fig. B.1

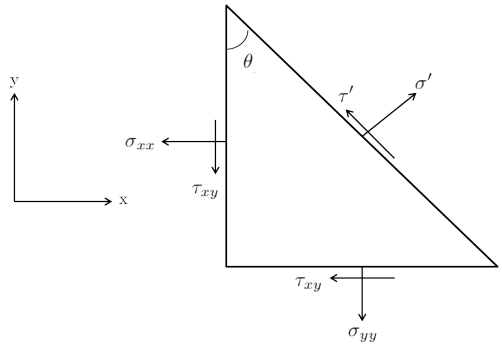

Figure B.1: *2D case with definitions.*

Using figure B.1 and summing the forces in x and y directions gives

$$\sigma' = \sigma_{xx}cos^2(\theta) + \sigma_{yy}sin^2(\theta) + 2\tau_{xy}cos(\theta)sin(\theta)$$
$$\tau' = (\sigma_{yy} - \sigma_{xx})cos(\theta)sin(\theta) + \tau_{xy}(cos^2(\theta) - sin^2(\theta))$$

reformulating the equations to

$$\sigma'_{xx} = \sigma_{xx}cos^2(\theta) + \sigma_{yy}sin^2(\theta) + 2\tau_{xy}cos(\theta)sin(\theta)$$
$$\sigma'_{yy} = \sigma_{xx}cos^2(\theta) + \sigma_{yy}sin^2(\theta) - 2\tau_{xy}cos(\theta)sin(\theta)$$
$$\tau'_{xy} = (\sigma_{yy} - \sigma_{xx})cos(\theta)sin(\theta) + \tau_{xy}(cos^2(\theta) - sin^2(\theta))$$

or in matrix format

$$\begin{bmatrix} \sigma'_{xx} & \tau'_{xy} \\ \tau'_{xy} & \sigma'_{yy} \end{bmatrix} = \begin{bmatrix} cos(\theta) & sin(\theta) \\ -sin(\theta) & cos(\theta) \end{bmatrix} \begin{bmatrix} \sigma_{xx} & \tau_{xy} \\ \tau_{xy} & \sigma_{yy} \end{bmatrix} \begin{bmatrix} cos(\theta) & -sin(\theta) \\ sin(\theta) & cos(\theta) \end{bmatrix}$$

i.e. $\boldsymbol{\sigma'} = \mathbf{A}\ \boldsymbol{\sigma}\ \mathbf{A}^T$, where $\mathbf{A}$ is the rotation matrix. For uni-axial loading the tensor $\boldsymbol{\sigma}$ becomes

$$\boldsymbol{\sigma} = \begin{bmatrix} \sigma_\alpha & 0 \\ 0 & 0 \end{bmatrix}$$

where α is the material direction. Figure B.2 show this loading case.

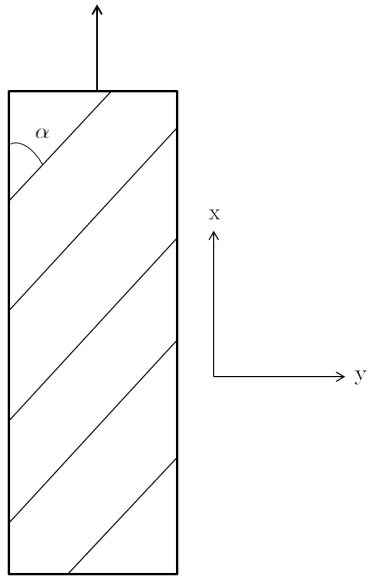

Figure B.2: *Uni-axial loading showing material direction α.*

C

Python script, Calculations.py

```
# Import Python packages
import pylab
import numpy as np
import matplotlib
from matplotlib.pyplot import *
from pylab import *
from scipy.integrate import simps, trapz
from collections import OrderedDict
from numpy.lib.scimath import sqrt

close("all")

# ============================================================

print("""
------------------------------------------------------------
Calculation file
Purpose: Calculating key values, plot different curves and yield surfaces.

Tetra Pak, Spring 2015
Tensile tests for aluminium-foil
Measured thickness = 9 my

The data is represented in angles where 0 is RD and 90 is TD.
------------------------------------------------------------
""")
# ============================================================

# maxDisp = int('max extension')
maxDisp = 9
# alpha = array('angles of the test')
alpha = [0, 10, 20, 30, 40, 45, 50, 60, 70, 80, 90]

# Import the median curves
Data = {}
```

```
for i in range(0,2*size(alpha),2):
    Data[i] = []
    Data[i+1] = []
    f = open('median_all.txt','r')
    for line in f:
        temp = line.split('\t')
        if temp[i][0].isdigit() == True:
            if float(temp[i])<maxDisp:
                Data[i].append(float(temp[i]))
                Data[i+1].append(float(temp[i+1]))

    f.close()

#-------------------------------------------------------
# Calculations

#----- Area for median curves -----
print '-----------------------------------------'
print 'Calculated area for mean curves using trapezoidal rule. The area is in
    [J/mm3].'
print 'Note that the area depends on the variable "maxDisp".'
print ''
Area = []
maxStrain = []
ind = 0
for j in range(0,2*size(alpha),2):
    maxStrain.append(float(Data[j][Data[j+1].index(max(Data[j+1]))]))
    area = trapz(np.asarray(Data[j+1])/(15*9e-3),Data[j])*0.01
    print 'Area for direction ' + str(alpha[ind]) + ' =', area
    ind += 1
    Area.append(float(area))
print ''
maxA = max(Area)
maxS = max(maxStrain)

print 'Max strain', maxStrain
print ''


#----- Maximum tensile stress surface -----

maxTensileStress = []
for i in range(0,2*size(alpha),2):
    maxTensileStress.append(float(max(Data[i+1])/(15*9e-3)))

maxTS = max(maxTensileStress)

print 'Ultimate tensile strength', maxTensileStress
print ''
```

```
# ------ E-modulus for each direction ------

print '-----------------------------------------'
print 'Youngs modulus for each direction in [GPa].'
print ''

E = []
ind = 0
for i in range(0,2*size(alpha),2):
    y1 = Data[i+1][2]/(15e-3*9e-6)
    y2 = Data[i+1][0]/(15e-3*9e-6)
    x1 = Data[i][2]*1e-2 # since it's in %
    x2 = Data[i][0]*1e-2

    E.append(float(((y2-y1)/(x2-x1))*1e-9))
    print 'Youngs modulus for direction ' + str(alpha[ind]) + ' =', E[ind]
    ind += 1
print ''

E_avg = sum(E)/size(E)
print 'Average Youngs modulus =', E_avg
print ''


# ------ Yield stress ------

yieldStress = []
yieldStrain = []

def f(x,E):
    return E*(x-0.2) # 0.2% Offset

index = 0
for i in range(0,2*size(alpha),2):
    (val,ind) = min((V,I) for I,V in enumerate(abs(Data[i+1] - f(array(Data[i
        ]),E_avg))))
    yieldStress.append(float(Data[i+1][ind]/(15*9e-3)))
    yieldStrain.append(float(Data[i][ind]))
    index += 1

maxY = max(yieldStress)

print 'Yield stress from 0 to 90 degree'
print yieldStress
print ''
print 'Yield strain from 0 to 90 degree'
print yieldStrain
print ''


# ------ Yield surface ------
```

```
sigY = maxTensileStress[0]
sigX = maxTensileStress[10]
print '[sigmaRD_max sigmaTD_max] =',sigY,sigX
print ''
sigy = yieldStress[0]
sigx = yieldStress[10]
print '[sigmaRD_y sigmaTD_y] =',sigy,sigx
print ''

x1 = arange(-1.3,-1.01,0.00001)
x2 = arange(-1.01,1.01,0.01)
x3 = arange(1.01,1.3,0.00001)
X = concatenate((x1,x2,x3),axis=0)

# Von Mises
M1 = []
M2 = []
XvM = []
for i in X:
    d = (sigx*i)**2 - sigx**2
    if real(sqrt((i*sigx)**2/4 - d)) > 0:
        XvM.append(float(i))
        M1.append(float(i*sigx/2 + sqrt((i*sigx)**2/4 - d)))
        M2.append(float(i*sigx/2 - sqrt((i*sigx)**2/4 - d)))
XvM = np.asarray(XvM)


# Calibration
y1 = yieldStress[0] # RD
y2 = yieldStress[10] # TD
y12 = yieldStress[5] # 45

F = 1./y2**2 - 1./(2*y1**2)
G = H = 1./(2*y1**2)
N = 2./y12**2 - 1./(2*y2**2)

def sigAlpha(a):
    return sqrt(1./((F+H)*cos(a*pi/180)**4 + (G+H)*sin(a*pi/180)**4 + 2*(N-H)*
        sin(a*pi/180)**2*cos(a*pi/180)**2))

Y1 = maxTensileStress[0] # RD
Y2 = maxTensileStress[10] # TD
Y12 = maxTensileStress[5] # 45

G2 = 1./Y1**2 - 1./(2*Y2**2)
F2 = H2 = 1./(2*Y2**2)
N2 = 2./Y12**2 - 1./(2*Y1**2)

def sigAlpha2(a):
    return sqrt(1./((F2+H2)*cos(a*pi/180)**4 + (G2+H2)*sin(a*pi/180)**4 + 2*(
```

```
        N2-H2)*sin(a*pi/180)**2*cos(a*pi/180)**2))


Hilly1 = []
Hilly2 = []
Hillx = []
for i in X:
    A = (2*H*y2*i)/(G+H)
    B = ((F+H)*(y2*i)**2 - 1)/(G+H)
    if real(sqrt(A**2/4 - B)) > 0:
        Hillx.append(float(i))
        Hilly1.append(float(A/2 + sqrt(A**2/4 - B)))
        Hilly2.append(float(A/2 - sqrt(A**2/4 - B)))
Hillx = np.asarray(Hillx)

Fm = 1./(sigX)**2 - 1./(2*sigY**2)
Gm = Hm = 1./(2*sigY**2)

HillY1 = []
HillY2 = []
HillX = []
for i in X:
    A = (2*Hm*sigX*i)/(Gm+Hm)
    B = ((Fm+Hm)*(sigX*i)**2 - 1)/(Gm+Hm)
    if real(sqrt(A**2/4 - B)) > 0:
        HillX.append(float(i))
        HillY1.append(float(A/2 + sqrt(A**2/4 - B)))
        HillY2.append(float(A/2 - sqrt(A**2/4 - B)))
HillX = np.asarray(HillX)


# ------------------------------------------------------------
# Plot settings

import matplotlib
matplotlib.rc('xtick', labelsize=30)
matplotlib.rc('ytick', labelsize=30)
plt.rc('text',usetex=True)
plt.rc('font',family='serif')
close()

angles_order = [0, 10, 20, 80, 90, 70, 30, 60, 50, 45, 40]
plot_order = [0, 1, 2, 9, 10, 8, 3, 7, 6, 5, 4]
colorcycle = ['blue', 'green', 'lime', 'cyan','magenta','red' ,'yellow','gray'
    ,'coral','maroon','black']
label_vec = ['RD', '10', '20', '30', '40', '45', '50', '60', '70', '80', 'TD']


# ------------------------------------------------------------
# Plots
```

```
# ----- Key values (normilized with max-value) -----
fig1 = plt.figure(num=1,figsize=(18, 9))
ax1 = fig1.add_subplot(111)
for i in range(0,size(alpha)):
    plot(alpha[i],yieldStress[i]/maxY,'ko',markersize=9,label='Yield Stress')
    plot(alpha[i],maxTensileStress[i]/maxTS,'b^',markersize=9,label='UTS')
    plot(alpha[i],Area[i]/maxA,'rv',markersize=9,label='TA energy')
    plot(alpha[i],maxStrain[i]/maxS,'gs',markersize=9,label='Max Strain')

pylab.title('Key values',fontsize=24)
ax1.set_xlabel('Angles [deg]',fontsize=30)
ax1.set_ylabel('Y/Y_{max}',fontsize=30)
pylab.grid(b=True,axis='both',which='major')
axes = plt.gca()
axes.set_ylim([0.4,1.1])
handles, labels = ax1.get_legend_handles_labels()
by_label = OrderedDict(zip(labels, handles))
legend(by_label.values(), by_label.keys(),numpoints=1,bbox_to_anchor=(1, 1),
    loc=1)

savefig('Key_values', dpi=None, facecolor='w', edgecolor='w',
            orientation='portrait', papertype=None, format=None,
            transparent=False)
show()



# ----- RD, TD and 45 directions -----
fig2 = plt.figure(num=2,figsize=(18, 9))
ax2 = fig2.add_subplot(111)

plot(Data[0],Data[1],'b',linewidth=2,label='RD')
plot(Data[20],Data[21],'k',linewidth=2,label='TD')
plot(Data[10],Data[11],'r',linewidth=2,label='45')

pylab.title('RD, TD and 45$^{\circ}$',fontsize=24)
ax2.set_xlabel('Displacement [mm]',fontsize=30)
ax2.set_ylabel('Force [N]',fontsize=30)
pylab.grid(b=True,axis='both',which='major')
axes = plt.gca()
axes.set_xlim([0,8])
axes.set_ylim([0,11])

savefig('Material_directions', dpi=None, facecolor='w', edgecolor='w',
            orientation='portrait', papertype=None, format=None,
            transparent=False)
show()



# ----- Yield surfaces -----
```

```
new_fig3 = plt.figure(num=3,figsize=(14, 14))
ax3 = new_fig3.add_subplot(111)

# Hill
plot(sigx*Hillx,Hilly1,'b',label='Hill')
plot(sigx*Hillx,Hilly2,'b')

# Von Mises
plot(sigx*XvM,M1,'k',label='Von Mises')
plot(sigx*XvM,M2,'k')

pylab.title('Yield surfaces',fontsize=24)
pylab.grid(b=True,axis='both',which='major')
ax3.set_xticks([])
ax3.set_yticks([])
ax3.spines['left'].set_position('zero')
ax3.spines['bottom'].set_position('zero')
ax3.xaxis.set_label_coords(0.95,0.5)
ax3.yaxis.set_label_coords(0.5,0.95)
ax3.set_xlabel(r'$\sigma_2$',fontsize=30)
ax3.set_ylabel(r'$\sigma_1$',fontsize=30)
handles, labels = ax3.get_legend_handles_labels()
by_label = OrderedDict(zip(labels, handles))
legend(by_label.values(), by_label.keys(),bbox_to_anchor=(0.8, 0.2),loc=2)

savefig('Yield_surfaces', dpi=None, facecolor='w', edgecolor='w',
            orientation='portrait', papertype=None, format=None,
            transparent=False)
show()



# ----- Isotropic hardening -----
new_fig4 = plt.figure(num=4,figsize=(14, 14))
ax4 = new_fig4.add_subplot(111)

# For yielding
plot(sigx*Hillx,Hilly1,'b',label='Yield')
plot(sigx*Hillx,Hilly2,'b')

# For fracture
plot(sigX*HillX,HillY1,'r',label='Fracture')
plot(sigX*HillX,HillY2,'r')

pylab.title('Hill surfaces',fontsize=24)
pylab.grid(b=True,axis='both',which='major')
ax4.set_xticks([])
ax4.set_yticks([])
ax4.spines['left'].set_position('zero')
ax4.spines['bottom'].set_position('zero')
ax4.xaxis.set_label_coords(0.96,0.5)
```

```
ax4.yaxis.set_label_coords(0.5,0.95)
ax4.set_xlabel(r'$\sigma_{TD}$',fontsize=30)
ax4.set_ylabel(r'$\sigma_{RD}$',fontsize=30)
handles, labels = ax4.get_legend_handles_labels()
by_label = OrderedDict(zip(labels, handles))
legend(by_label.values(), by_label.keys(),bbox_to_anchor=(0.8, 0.2),loc=2)

savefig('Isotropic_hardening', dpi=None, facecolor='w', edgecolor='w',
            orientation='portrait', papertype=None, format=None,
            transparent=False)
show()



# ------ Hill compared to experimental ------
new_fig5 = plt.figure(num=5,figsize=(18, 9))
ax5 = new_fig5.add_subplot(111)

for i in range(0,size(alpha)):
    plot(alpha[10-i],yieldStress[10-i],'ro',markersize=10,label='Experimental
        values (yield)')
    plot(alpha[10-i],sigAlpha(alpha[i]),'k-',markersize=8,label='Hill model (
        yield)')

    plot(alpha[10-i],maxTensileStress[10-i],'go',markersize=10,label='
        Experimental values (fracture)')
    plot(alpha[10-i],sigAlpha2(alpha[i]),'b-',markersize=8,label='Hill model (
        fracture)')


for i in arange(0,90,0.1):
    plot(90-i,sigAlpha(i),'ko',markersize=1)
    plot(90-i,sigAlpha2(i),'bo',markersize=1)

pylab.title('Hill compared to experimental',fontsize=24)
ax5.set_xlabel('$Angles$ $[deg]$',fontsize=30)
ax5.set_ylabel('$\sigma_y$ $[MPa]$',fontsize=30)
pylab.grid(b=True,axis='both',which='major')
axes = plt.gca()
axes.set_ylim([30,80])
handles, labels = ax5.get_legend_handles_labels()
by_label = OrderedDict(zip(labels, handles))
legend(by_label.values(), by_label.keys(),numpoints=1)

savefig('Hill_compared_to_experimental', dpi=None, facecolor='w', edgecolor='w
    ',
            orientation='portrait', papertype=None, format=None,
            transparent=False)

show()
```